MAMBASL: EXPLORING SINGLE-LAYER MAMBA FOR TIME SERIES CLASSIFICATION

Yoo-Min Jung & Leekyung Kim
Department of Industrial Engineering, Seoul National University
pamela7384@gmail.com, klk97@snu.ac.kr

ABSTRACT

Despite recent advances in state space models (SSMs) such as Mamba across various sequence domains, research on their standalone capacity for time series classification (TSC) has remained limited. We propose MambaSL, a framework that minimally redesigns the selective SSM and projection layers of a *single-layer Mamba*, guided by four TSC-specific hypotheses. To address benchmarking limitations—restricted configurations, partial University of East Anglia (UEA) dataset coverage, and insufficiently reproducible setups—we re-evaluate 20 strong baselines across all 30 UEA datasets under a unified protocol. As a result, MambaSL achieves state-of-the-art performance with statistically significant average improvements, while ensuring reproducibility via public checkpoints for all evaluated models. Together with visualizations, these results demonstrate the potential of Mamba-based architectures as a TSC backbone.

1 INTRODUCTION

State space models (SSMs) have emerged as a strong alternative to Transformers (Vaswani et al., 2017), with Mamba (Gu & Dao, 2024; Dao & Gu, 2024) marking a milestone in sequence domains such as language and video (Lenz et al., 2025; Li et al., 2024). In time series, however, convolutional- and Transformer-based architectures still dominate, with the former excelling in time series classification (TSC) and the latter in time series forecasting (TSF) (Wang et al., 2024b). While early works such as TimeMachine (Ahamed & Cheng, 2024) and S-Mamba (Wang et al., 2025b) showed Mamba's promise in TSF, its role in TSC remains underexplored.

Two gaps motivate our study. First, the standalone capacity of Mamba for TSC has seen little investigation. Wang et al. (2024b) ranked Mamba as the weakest TSC backbone, likely due to a lack of research rather than inherent architectural limitations, as only the vanilla variant was evaluated. To the best of our knowledge, TSCMamba (Ahamed & Cheng, 2025) is the only subsequent benchmarking attempt for TSC. However, its integration of feature engineering techniques such as ROCKET (Dempster et al., 2020) and CWT (Mallat, 1999) obscures Mamba's intrinsic contribution.

As a second gap, current TSC benchmarking suffers from three critical issues related to coverage, fairness, and reproducibility. First, evaluations are often restricted to only a fraction of the University of East Anglia (UEA) archive (Bagnall et al., 2018), leaving out challenging datasets with long sequences or high input dimensionality. Second, non-TSC models are frequently adopted without proper re-tuning, which risks underestimating their capacity; for example, TSF models like DLinear (Zeng et al., 2023) and PatchTST (Nie et al., 2023) have been reported in TSC contexts using default settings (Wu et al., 2023; Luo & Wang, 2024). Finally, reproducibility remains a concern—e.g., re-evaluations of TS2Vec (Yue et al., 2022) and GPT4TS (Zhou et al., 2023) by Eldele et al. (2024) revealed average accuracy drops exceeding 9%p compared to their original reports. These limitations undermine the reliability of comparative conclusions in the literature.

Motivated by these gaps, we revisit Mamba as a TSC backbone from two perspectives. **(i) Architecture:** We propose four TSC-specific hypotheses (H1–H4), which guide the redesign of selective SSM components and the input and output projection layers. **(ii) Evaluation protocol:** We establish a consistent benchmarking setup and re-evaluate strong TSC baselines across all 30 multivariate UEA datasets with extensive hyperparameter sweeps. Under the protocol, our *single-layer Mamba* TSC framework, MambaSL, achieves state-of-the-art performance. Our key contributions are:

- **TSC-specific hypotheses and architectural refinements.** We propose the following four hypotheses (H1–H4) that explain why naively applying Mamba within the existing TSC pipeline does not fully realize its potential, and validate them through corresponding design adjustments:
  - **(H1) Scale input projection.** Since Mamba's output is modulated by a gating unit (Hua et al., 2022; Mehta et al., 2023a), insufficient input context can bottleneck performance, motivating a larger input projection receptive field for densely sampled time series.
  - **(H2) Modularize time (in)variance.** As time series often exhibit near linear time-invariant behavior, we decouple time variance of Mamba as a hyperparameter. Simpler configurations often perform better, contradicting the ablation results from Gu & Dao (2024).
  - **(H3) Remove skip connection.** In shallow networks, skip connections yield minimal performance gains (He et al., 2016; Ismail Fawaz et al., 2020). Given Mamba's strong long-range memory, we remove skip connections and construct logits solely from hidden states.
  - **(H4) Aggregate via adaptive pooling.** Time series classification spans both global and event-driven patterns, which conventional pooling cannot accommodate. We therefore propose a multi-head adaptive pooling that weights temporal features in a dataset-specific manner.
- **Comprehensive and reproducible UEA benchmarking.** We evaluate 20 models on all 30 UEA datasets, covering various sequence lengths (8–17,984), input dimensions (2–1,345), and sample sizes (12–25,000). For each model, we explore approximately 200 hyperparameter combinations to select the optimal configuration. Notably, TSF models previously tested on the UEA datasets showed an average accuracy improvement of 3.04%p with hyperparameter tuning alone.
- **Empirical validation of a single-layer Mamba.** Our MambaSL framework achieves the state-of-the-art performance across the UEA benchmark, outperforming the second-best method by 1.41%p. We demonstrate the inherent potential of Mamba by validating our hypotheses through ablation studies and highlighting backbone- and dataset-specific features through visualizations.

The remainder of the paper is organized as follows. Section 2 reviews related work for TSC and Mamba, section 3 details our hypotheses and architectural refinements, section 4 describes our experimental setup and implementation details, section 5 presents results and analysis, and section 6 concludes the paper.

2 Related work

Recent advances in deep learning (DL) for TSC can be grouped into three streams. (i) **TSC-specific models** such as TS2Vec tailor encoders and readouts directly for classification (Yue et al., 2022; Eldele et al., 2024; Wen et al., 2025). (ii) **Foundation models** aim to adapt a single model across multiple time-series tasks, including TSC (Wu et al., 2023; Zhou et al., 2023; Luo & Wang, 2024; Wang et al., 2025a). (iii) **TSF-origin models** are frequently repurposed as baselines for TSC-specific and foundation models (Zeng et al., 2023; Zhang & Yan, 2023; Nie et al., 2023). Although evaluations typically rely on the UEA benchmark, inconsistent use of dataset subsets and single-setting evaluations for TSF-origin models have led to underestimated baselines. This highlights the need for standardized and consistent benchmarking in TSC.

Within SSMs, Mamba has been explored primarily for TSF. Variants such as TimeMachine (Ahamed & Cheng, 2024) and S-Mamba (Wang et al., 2025b) typically construct temporally mixed embeddings and then apply bidirectional Mamba along the channel axis to mitigate scan-order sensitivity. By contrast, adaptations to TSC in general are comparatively scarce, with TSCMamba (Ahamed & Cheng, 2025) being the only variant. Across TSF and TSC alike, Mamba variants tend to update the SSM state along non-temporal axes (channel or frequency) rather than the original time axis.

3 Methods

3.1 Problem Definition

Let $\boldsymbol{X} = \boldsymbol{x}_{1:L} = [\boldsymbol{x}_1; \ldots; \boldsymbol{x}_L]$ be a multivariate time series of length L, where each x_t at time t is a d_{x}-D vector. TSC infers the label $y \in \{1, \ldots, d_{\mathrm{y}}\}$ from $\boldsymbol{X}$, where d_{y} is the number of classes.

Many TSC architectures consist of three fundamental modules: an input projection Φ_{I} that maps the input subsequence $\boldsymbol{x}_{t-k+1:t}$ (receptive field of size k) into a d_{m}-D vector $\tilde{\boldsymbol{x}}_t = [\,\tilde{x}_t^{(1)}, \ldots, \tilde{x}_t^{(d_{\mathrm{m}})}\,]$, a feature extractor Φ_{FE} that produces per-timestep feature vectors $\boldsymbol{f}_{1:L}$ from $\tilde{\boldsymbol{x}}_{1:L}$ (typically of the same size), and an output projection Φ_{CLF} that aggregates $\boldsymbol{f}_{1:L}$ into logits $\boldsymbol{l} \in \mathbb{R}^{d_{\text{y}}}$. Formally,

$$\begin{aligned} \tilde{\boldsymbol{x}}_t &= \Phi_{\text{I}}\big(\boldsymbol{x}_{t-k+1:t}\big), && (1)\\ \boldsymbol{f}_{1:L} &= \Phi_{\text{FE}}\big(\tilde{\boldsymbol{x}}_{1:L}\big), && (2)\\ \boldsymbol{l} &= \Phi_{\text{CLF}}\big(\boldsymbol{f}_{1:L}\big), && (3)\\ \hat{y} &= \underset{i \in \{1,\ldots,d_{\text{y}}\}}{\arg\max}\ \operatorname{softmax}(\boldsymbol{l})_i. && (4) \end{aligned}$$

The aggregation function of Φ_{CLF} can be instantiated as a fully connected layer, global average/max pooling, or a last-timestep readout. Whereas many recent studies primarily emphasize improving Φ_{FE}, we examine and improve the entire TSC pipeline for Mamba in section 3.3.

3.2 Time-variant SSM in Mamba

At a high level, Mamba can be viewed as a selective SSM core augmented with a lightweight gated linear block (Hua et al., 2022; Mehta et al., 2023a). We next review the selective SSM, clarifying its components and establishing the notation used in our proposed method (section 3.3.2).

3.2.1 Linear time-invariant SSM

An SSM maps a signal $u(t) \in \mathbb{R}$ to a d_{s}-D state vector $\boldsymbol{s}(t)$ and projects it onto an output $y(t) \in \mathbb{R}$:

$$\dot{\boldsymbol{s}}(t) = \boldsymbol{A}\boldsymbol{s}(t) + \boldsymbol{B}u(t), \qquad y(t) = \boldsymbol{C}\boldsymbol{s}(t) + \boldsymbol{D}u(t), \tag{5}$$

with four parameters, $\boldsymbol{A} \in \mathbb{R}^{d_{\text{s}} \times d_{\text{s}}}$, $\boldsymbol{B} \in \mathbb{R}^{d_{\text{s}} \times 1}$, $\boldsymbol{C} \in \mathbb{R}^{1 \times d_{\text{s}}}$, and $\boldsymbol{D} \in \mathbb{R}$. This yields a linear time-invariant (LTI) system when the parameters are fixed over time.

With a step size $\Delta > 0$, the system is discretized as

$$\boldsymbol{s}_t = \bar{\boldsymbol{A}}\boldsymbol{s}_{t-1} + \bar{\boldsymbol{B}}u_t, \qquad y_t = \boldsymbol{C}\boldsymbol{s}_t + \boldsymbol{D}u_t, \tag{6}$$

where $\bar{\boldsymbol{A}} = \mathcal{F}_A(\Delta, \boldsymbol{A})$ and $\bar{\boldsymbol{B}} = \mathcal{F}_B(\Delta, \boldsymbol{A}, \boldsymbol{B})$ are discretization rules. Different discretization rules exist; the zero-order hold (ZOH) method is discussed in section 3.2.2.

While these forms are standard, we retain them here as the basis for our *multivariate* extension. In SSM-based DL models, this extension is typically implemented by sharing $\boldsymbol{A}$ across channels and broadcasting the other parameters (Gu et al., 2021; 2022; Gu & Dao, 2024). For instance, when using the SSM as the feature extractor Φ_{FE} in equation 2, each input channel $\tilde{x}_t^{(j)}$ is mapped to a d_{s}-D state via channel-specific $\boldsymbol{B}^{(j)}$ (and step size $\Delta^{(j)}$) and shared $\boldsymbol{A}$. Thus, at time t, the hidden state $\boldsymbol{S}_t = [\,\boldsymbol{s}_t^{(1)}; \ldots; \boldsymbol{s}_t^{(d_{\text{m}})}\,] \in \mathbb{R}^{d_{\text{s}} \times d_{\text{m}}}$ where $\boldsymbol{s}_t^{(j)} = \mathcal{F}_A(\Delta^{(j)}, \boldsymbol{A})\boldsymbol{s}_{t-1}^{(j)} + \mathcal{F}_B(\Delta^{(j)}, \boldsymbol{A}, \boldsymbol{B}^{(j)})\tilde{x}_t^{(j)}$. The feature vector $\boldsymbol{f}_t$ is also generated by channel-specific $\boldsymbol{C}^{(j)}$ and $\boldsymbol{D}^{(j)}$. That is, in DL practice, the multivariate SSM is fundamentally a channel-independent LTI system.

To our knowledge, however, existing works rarely formalize how Δ, $\boldsymbol{B}$, and $\boldsymbol{C}$ operate across channels. We show explicitly that Δ primarily acts along the temporal axis on each channel, whereas $\boldsymbol{B}$ and $\boldsymbol{C}$ primarily serve as channel-wise projections under a shared $\boldsymbol{A}$ in Mamba's selective SSM. This clarification, often left implicit in prior literature, sets the stage for the following section.

3.2.2 Selective SSM

Mamba (Gu & Dao, 2024) proposed a selective SSM that allows Δ, $\boldsymbol{B}$, and $\boldsymbol{C}$ to selectively propagate or forget information from given input. Given the projected input $\tilde{\boldsymbol{x}}_t \in \mathbb{R}^{d_{\text{m}}}$, three learnable maps, ϕ_Δ, $\phi_{\boldsymbol{B}}$, and $\phi_{\boldsymbol{C}}$, produce the input-dependent parameters $\boldsymbol{\Delta}_t$, $\boldsymbol{B}_t$, and $\boldsymbol{C}_t$, respectively:

$$\begin{aligned} \boldsymbol{\Delta}_t &= \phi_\Delta(\tilde{\boldsymbol{x}}_t) = \zeta\big(\operatorname{Linear}^{\text{bias}}_{d_{\text{m}}}\big(\operatorname{Linear}_{d_{\text{r}}}(\tilde{\boldsymbol{x}}_t)\big)\big) = (\Delta_t^{(1)}, \ldots, \Delta_t^{(d_{\text{m}})}) && \in \mathbb{R}^{d_{\text{m}}}_{>0},\\ \boldsymbol{B}_t &= \phi_B(\tilde{\boldsymbol{x}}_t) = \operatorname{Linear}_{d_{\text{s}}}(\tilde{\boldsymbol{x}}_t) && \in \mathbb{R}^{d_{\text{s}} \times 1},\\ \boldsymbol{C}_t &= \phi_C(\tilde{\boldsymbol{x}}_t) = \operatorname{Linear}_{d_{\text{s}}}(\tilde{\boldsymbol{x}}_t)^\top && \in \mathbb{R}^{1 \times d_{\text{s}}}. \end{aligned} \tag{7}$$

Here, ζ is the softplus activation, $\operatorname{Linear}^{\text{bias}}_d(x)$ and $\operatorname{Linear}_d(x)$ denote linear projections into $\mathbb{R}^d$ (identified with $\mathbb{R}^{d \times 1}$) with and without bias, and d_{r} is the rank of low-rank projection for $\boldsymbol{\Delta}_t$.

The selective SSM is then formulated as follows:[1]

$$\boldsymbol{s}_t^{(j)} = \bar{\boldsymbol{A}}_t^{(j)} \boldsymbol{s}_{t-1}^{(j)} + \bar{\boldsymbol{B}}_t^{(j)} \tilde{x}_t^{(j)}, \qquad f_t^{(j)} = \boldsymbol{C}_t \boldsymbol{s}_t^{(j)} + \boldsymbol{D}^{(j)} \tilde{x}_t^{(j)}, \quad j = 1, \ldots, d_{\mathrm{m}}, \tag{8}$$

where $\bar{\boldsymbol{A}}_t^{(j)}$ and $\bar{\boldsymbol{B}}_t^{(j)}$ are discretized by the ZOH rule (Mehta et al., 2023b; Gu & Dao, 2024):

$$\begin{aligned} \bar{\boldsymbol{A}}_t^{(j)} &= \mathcal{F}_A(\Delta_t^{(j)}, \boldsymbol{A}) = \exp(\Delta_t^{(j)} \boldsymbol{A}), \\ \bar{\boldsymbol{B}}_t^{(j)} &= \mathcal{F}_B(\Delta_t^{(j)}, \boldsymbol{A}, \boldsymbol{B}_t) = (\Delta_t^{(j)} \boldsymbol{A})^{-1} (\exp(\Delta_t^{(j)} \boldsymbol{A}) - \boldsymbol{I}) \Delta_t^{(j)} \boldsymbol{B}_t. \end{aligned} \tag{9}$$

This transformation changes the SSM from an LTI to a time-variant (TV) system, enabling context-aware reasoning that selectively stores or extracts key information. The explicit formulation also highlights that $\boldsymbol{A}$, $\boldsymbol{B}_t$, and $\boldsymbol{C}_t$ are shared across channels, while $\bar{\boldsymbol{A}}_t^{(j)}$ and $\bar{\boldsymbol{B}}_t^{(j)}$ differ due to the channel-wise $\Delta_t^{(j)}$.

3.2.3 On time variance in Δ, $\boldsymbol{B}$, and $\boldsymbol{C}$

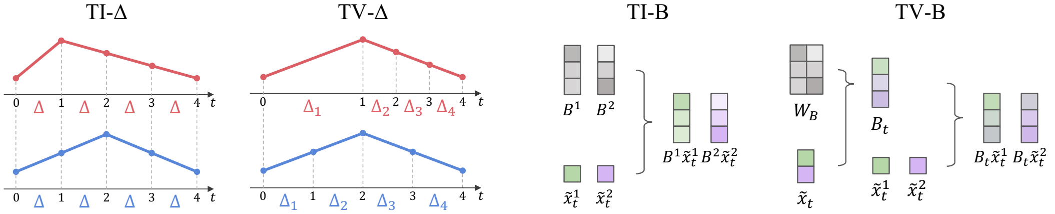

Figure 1: TI/TV parameterization of (left) Δ and (right) $\boldsymbol{B}$ in the SSM. TI-Δ fixes the update rate, while TV-Δ adapts it to align sequences with varying speeds. TI-$\boldsymbol{B}$ preserves channel independence, whereas TV-$\boldsymbol{B}$ introduces input-dependent mixing. $\boldsymbol{C}$ follows the same pattern as $\boldsymbol{B}$ at the output stage, highlighting the temporal pacing of Δ versus the spatial routing of $\boldsymbol{B}$ and $\boldsymbol{C}$.

While the parameters in Mamba share the same mechanism to yield a TV system by default, as defined in equation 7, their main roles differ. We denote Δ, $\boldsymbol{B}$, and $\boldsymbol{C}$ in the LTI SSM using TI-notation (section 3.2.1), and $\boldsymbol{\Delta}_t$, $\boldsymbol{B}_t$, and $\boldsymbol{C}_t$ in the selective SSM using TV- notation (section 3.2.2).

Δ: Temporal Update Rate. Δ controls the timescale of state updates. TI-Δ keeps a constant rate, whereas TV-Δ adapts to context: larger Δ accelerates updates, and smaller Δ prolongs memory. This resembles dynamic time warping (DTW), aligning sequences with varying local speeds (see the left side of Figure 1).

$\boldsymbol{B}$: Input-to-State Routing. $\boldsymbol{B}$ determines how each input channel drives the latent state. TI-$\boldsymbol{B}$ enforces channel-independent routing, whereas TV-$\boldsymbol{B}$ enables context-dependent mixing of input channels before entering the state space (see the right side of Figure 1).

$\boldsymbol{C}$: State-to-Output Readout. $\boldsymbol{C}$ maps states to output features. TI-$\boldsymbol{C}$ applies a fixed readout, preserving channel independence. TV-$\boldsymbol{C}$ introduces adaptive mixing at the output stage, potentially capturing richer cross-channel interactions.

Interplay. TV-Δ governs *temporal dynamics*, whereas TV-$\boldsymbol{B}$ and TV-$\boldsymbol{C}$ govern *spatial mixing*. The extreme cases are:

- TI-Δ, TI-$\boldsymbol{B}$, TI-$\boldsymbol{C}$: LTI system with channel-independent I/O;
- TV-Δ, TV-$\boldsymbol{B}$, TV-$\boldsymbol{C}$: fully TV system with channel-mixed I/O.

Thus, temporal and spatial variability can be decoupled and selectively controlled, motivating our second hypothesis (H2) in section 3.3.2. Note that, while these roles are primary, the ZOH rule couples them to some extent: Δ can indirectly modulate the influence of $\boldsymbol{B}$ and $\boldsymbol{C}$, and vice versa.

3.3 Single-layer Mamba for TSC

We refine the vanilla Mamba and projection layers through four hypotheses (H1–H4) motivated by their limitations in the standard TSC pipeline. The full framework is shown in Figure 2.

[1] For simplicity, we treat the selective SSM without shift as the feature extractor itself, using $\tilde{\boldsymbol{x}}_t$ in place of u_t and $\boldsymbol{f}_t$ in place of y_t from equation 6. In practice, Δ, $\boldsymbol{B}$, and $\boldsymbol{C}$ are generated from an expanded input after a linear projection and a local convolution, but we omit this detail to keep the notation concise.

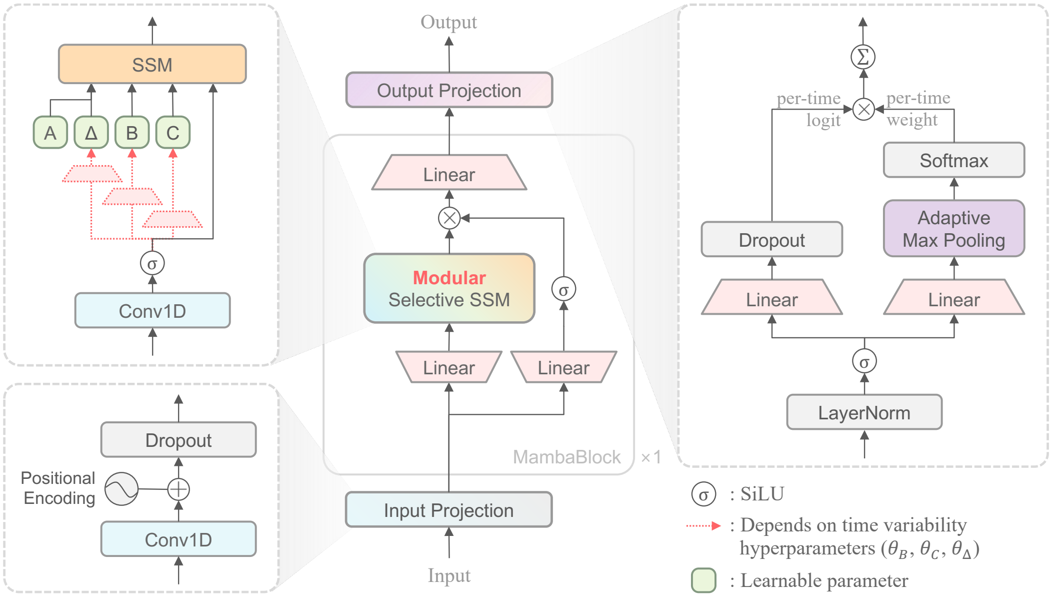

Figure 2: Overall structure of MambaSL, a single-layer Mamba framework designed for TSC.

3.3.1 Input Projection

H1: Scale input projection In recent time series models, Φ_{I} is implemented as a 1-D convolution with a fixed kernel size $k = 3$ (Wu et al., 2023; Zhou et al., 2023), unless alternatives such as patching or frequency-domain transforms are employed (Nie et al., 2023; Wang et al., 2025a).

Since Mamba's gating mechanism modulates the SSM output based on this projection, we hypothesize that longer sequences require proportionally larger receptive fields. We therefore define

$$k = \max(k_{\text{min}}, \lfloor \lambda L \rfloor), \tag{10}$$

with $k_{\text{min}} = 3$ (minimum k), $\lambda = 0.02$ (sequence ratio), and stride $= 1$ to isolate kernel-size effects.

3.3.2 Feature Extractor

We adopt the vanilla Mamba as our feature extractor, introducing minimal changes to its SSM core under two hypotheses: (H2) modularizing time (in)variance and (H3) removing the skip connection.

H2: Modularize time (in)variance Building on section 3.2.3, we hypothesize that the optimal TI/TV configuration of Δ, $\boldsymbol{B}$, and $\boldsymbol{C}$ is dataset-dependent. Evidence from TSF shows that channel independence may outperform mixing (Zeng et al., 2023; Nie et al., 2023), and shape-based distance—akin to TI-Δ—can rival DTW in TSC (Paparrizos & Gravano, 2015). As aggregation with channel mixing is inevitable at the output, we expect $\boldsymbol{C}$ to have a comparatively smaller effect, while Δ and $\boldsymbol{B}$ are likely to exert a larger dataset-specific influence.

To systematically examine this, we introduce binary switches $\theta_\Delta, \theta_{\boldsymbol{B}}, \theta_{\boldsymbol{C}} \in \{0, 1\}$ that determine whether each parameter follows a TI or TV form. For channel $j \in \{1, \ldots, d_{\text{m}}\}$ and time t, the effective parameters are

$$\begin{aligned}
\Delta_t^{(j)\star} &= (1-\theta_\Delta)\,\Delta^{(j)} + \theta_\Delta\,\Delta_t^{(j)} &&= (1-\theta_\Delta)\,\Delta^{(j)} + \theta_\Delta\,\phi_\Delta(\tilde{\boldsymbol{x}}_t)^{(j)} &&\in \mathbb{R}_{>0},\\
\boldsymbol{B}_t^{(j)\star} &= (1-\theta_{\boldsymbol{B}})\,\boldsymbol{B}^{(j)} + \theta_{\boldsymbol{B}}\,\boldsymbol{B}_t &&= (1-\theta_{\boldsymbol{B}})\,\boldsymbol{B}^{(j)} + \theta_{\boldsymbol{B}}\,\phi_{\boldsymbol{B}}(\tilde{\boldsymbol{x}}_t) &&\in \mathbb{R}^{d_s \times 1},\\
\boldsymbol{C}_t^{(j)\star} &= (1-\theta_{\boldsymbol{C}})\,\boldsymbol{C}^{(j)} + \theta_{\boldsymbol{C}}\,\boldsymbol{C}_t &&= (1-\theta_{\boldsymbol{C}})\,\boldsymbol{C}^{(j)} + \theta_{\boldsymbol{C}}\,\phi_{\boldsymbol{C}}(\tilde{\boldsymbol{x}}_t) &&\in \mathbb{R}^{1 \times d_s},
\end{aligned} \tag{11}$$

where all ϕ are defined in equation 7. This modularization yields $2^3 = 8$ configurations, ranging from a fully LTI system (all $\theta = 0$) to the selective SSM (all $\theta = 1$). Substituting equation 11 into equations 8 and 9 produces our modularized selective SSM, illustrated in the upper left of Figure 2.

H3: Remove skip connection Skip (residual) connections improve optimization in deep networks, yet their effect diminishes in shallow networks (He et al., 2016; Kim et al., 2017). InceptionTime (Ismail Fawaz et al., 2020) further shows that the skip connection makes little difference across 85 UCR datasets (Chen et al., 2015), indicating that it is not always essential for TSC.

In the single-layer setting, such shortcuts may bypass the SSM and hinder Mamba's representation learning. We therefore hypothesize that removing the skip connection forces the model to rely solely on the SSM's state evolution. This is implemented by omitting the $\boldsymbol{D}^{(j)}\tilde{x}_t^{(j)}$ term in equation 8 [2]:

$$f_t^{(j)} = \boldsymbol{C}_t \boldsymbol{s}_t^{(j)} \quad \text{(no skip term)}\,. \tag{12}$$

This modification positions learning the state vector $\boldsymbol{s}_t^{(j)}$ as the core of TSC.

3.3.3 Output projection

H4: Aggregate via adaptive pooling After the Mamba block, per-timestep features are aggregated into a logit vector $\boldsymbol{l}$. Conventional pooling methods, such as average or max, treat all steps equally or rely on a single dominant one, thus ignoring data-specific temporal importance. This issue is particularly critical for recurrent models, where the predicted label may shift over time (e.g., a `Handwriting` sequence labeled g may initially resemble class a before later aligning with g).

We propose a multi-head adaptive pooling with learnable gates (Figure 3). Specifically, N_h independent gating heads each produce a scalar score $g_{t,h}$ for time step t:

$$g_{t,h} = \boldsymbol{w}_h^\top \boldsymbol{f}_t + b_h, \quad h = 1, \ldots, N_h. \tag{13}$$

For each t, the maximum gate value across heads is selected and normalized via softmax to obtain per-timestep weight α_t, which is then applied to the per-timestep logit vector $\boldsymbol{l}_t$:

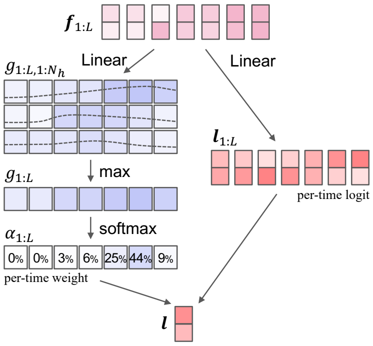

Figure 3: Illustration of proposed multi-head adaptive pooling with $(L, d_\mathrm{m}, N_h, d_\mathrm{y}) = (7, 2, 3, 2)$.

$$g_t = \max_h g_{t,h}, \qquad \alpha_t = \frac{\exp(g_t)}{\sum_{i=1}^{L} \exp(g_i)}, \qquad \boldsymbol{l} = \sum_{t=1}^{L} \alpha_t \boldsymbol{l}_t. \tag{14}$$

This formulation generalizes conventional pooling: uniform α_t recovers averaging, while a sharply peaked α_t approximates max pooling. Compared to attention pooling (Bahdanau et al., 2016), our design is lightweight yet expressive: multi-head gating explores diverse patterns, while adaptive max pooling selects the most confident signals, enabling robust dataset-specific aggregation.

4 Experiment

We conduct experiments on the full UEA benchmark (Bagnall et al., 2018), covering diverse sequence lengths, input dimensions, and sample sizes. For conciseness, we will hereafter refer to each dataset by its code (e.g., `EC` for EthanolConcentration; see Table 4). To ensure fairness, we allocate an identical search budget per model–dataset under a unified protocol, selecting the best configuration for each dataset. Detailed descriptions of the environment, datasets, and metrics are provided in appendix A, and hyperparameter settings are provided in appendix B.

Baselines We include (1) non-DL methods: DTW-based nearest neighbor (DTW$_D$; Berndt & Clifford, 1994), ROCKET (Dempster et al., 2020), HIVE-COTE 2.0 (HC2; Middlehurst et al., 2021), Hydra (Dempster et al., 2023), MultiRocket (MR; Tan et al., 2022)+Hydra; (2) MLP-based models: DLinear (Zeng et al., 2023), LightTS (Zhang et al., 2022), MTS-Mixer (Li et al., 2023); (3) CNN-based models: TimesNet (Wu et al., 2023), ModernTCN (Luo & Wang, 2024), TSLANet (Eldele et al., 2024), TimeMixer++ (Wang et al., 2025a); (4) Transformer-based models: FEDformer (Zhou et al., 2022), ETSformer (Woo et al., 2022), Crossformer (Zhang & Yan, 2023), PatchTST (Nie et al., 2023), GPT4TS (Zhou et al., 2023), iTransformer (Liu et al., 2024); (5) shape-based model: InterpGN (Wen et al., 2025); and (6) Mamba-based model: TSCMamba (Ahamed & Cheng, 2025).

[2] While Mamba and related literature typically derive the SSM equation without the skip connection $\boldsymbol{D}$, their official implementations default to enabling it (state-spaces, 2025). We changed this to be tunable.

5 RESULTS AND DISCUSSION

5.1 CLASSIFICATION RESULTS ON THE UEA BENCHMARK

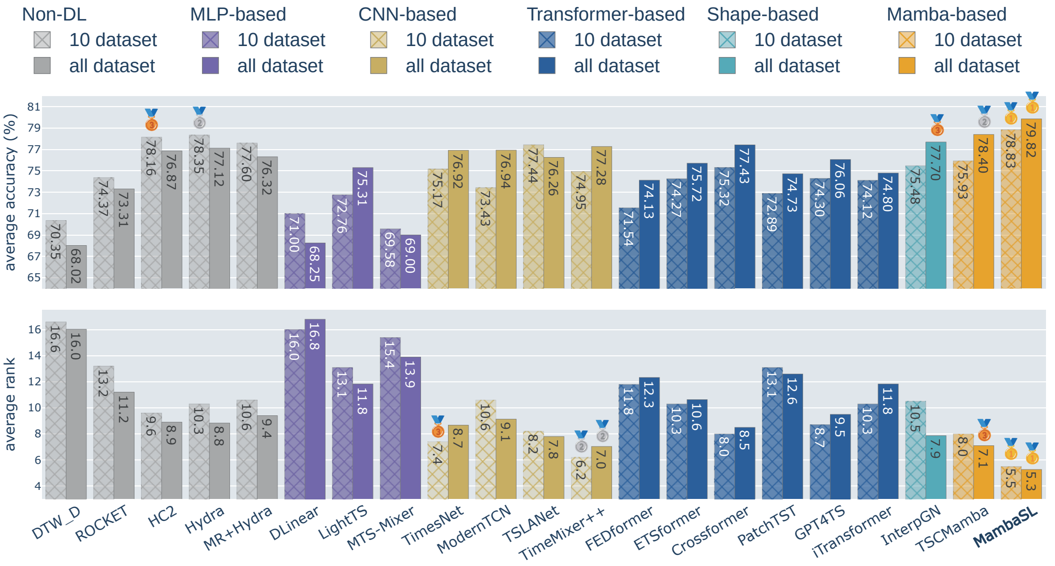

Figure 4: Comparison of average classification performances on the UEA benchmark. Non-DL models include DTW-D, ROCKET, HC2, Hydra, and MR+Hydra; DL models are grouped by their backbone structures.

As shown in Figure 4, our proposed model—MambaSL—established a new state of the art by achieving the best average accuracy and rank across both the widely used 10-dataset subset and the full set of 30 UEA datasets. In particular, MambaSL surpassed the second-best model, TSC-Mamba, by an average margin of 1.41%p. Wilcoxon signed-rank tests (Wilcoxon, 1945) across the 30 datasets confirmed statistically significant gains ($p < 0.05$) over all models except HC2 ($p = 0.56$), despite HC2 ranking only 8th overall (see appendix C.1 for full results and statistics).

As detailed in appendix C.1, MambaSL tends to perform strongly on datasets where multi-scale convolutions or frequency-domain features are typically dominant. For example, `AWR`, `CR`, `EW`, `EP`, `HW`, `PS`, `RS`, `UW`, and `SWJ` generally favor non-DL, TSLANet, InterpGN, and TSCMamba, yet MambaSL remains competitive. In particular, for `CR` and `HW`, MambaSL is the only DL model that surpasses DTW_D. At the same time, MambaSL shows competitive results on datasets such as `FD`, `HMD`, `NATO`, and `SRS1`, where MLP- or Transformer-based backbones have relative advantages. These results, achieved without additional domain transforms or complex mechanisms, demonstrate both the inherent capability of Mamba and the effectiveness of our architectural refinements.

To further contextualize the results, Figure 5 visualizes each model using a 2-D embedding of its 30 accuracy values via uniform manifold approximation and projection (UMAP) (McInnes et al., 2020). DL and non-DL methods are clearly clustered in separate regions, while InterpGN and MambaSL appear in between. The placement of InterpGN is reasonable since it ensembles shape-based and DL models. This suggests that MambaSL shares the strengths of both DL and non-DL approaches.

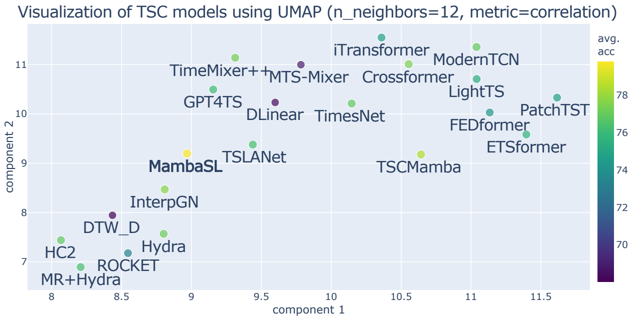

Figure 5: Visualization of the UEA classification results of each TSC model using the UMAP algorithm.

To complement the model-level analysis in Figure 5, we visualize the UEA datasets via UMAP in Figure 6. Here, each point represents a dataset embedded by its 21 accuracy values. Compared to the full results in appendix C.1, this view clearly shows the pattern of non-DL methods; datasets on which all non-DL baselines perform poorly form a tight cluster in the lower right (`FD`, `JV`, `SRS2`, `AF`, `FM`, `HMD`, `MI`, `SWJ`), whereas the upper-left cluster tends to outperform under the non-DLs.

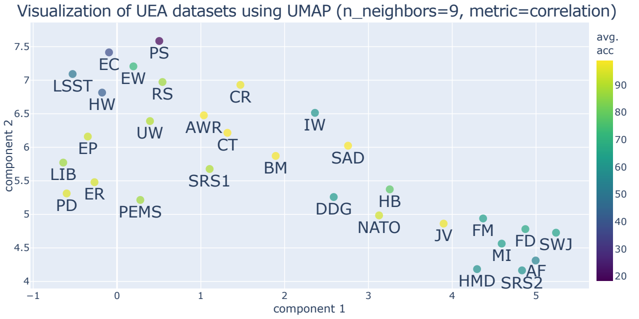

Figure 6: Visualization of the UEA classification results using the UMAP algorithm along dataset axis.

Finally, reproducibility remains a challenge in DL models due to randomness in initialization and optimization. We therefore compared our results with prior reports (appendix C.3). Our evaluation yielded higher performance than previously reported results, except for ModernTCN and TimeMixer++. However, their average ranks decline when the reported results are applied, confirming the fairness and rigor of our protocol across all baselines. For ModernTCN, although the average accuracy was lower than expected, we achieved higher accuracy with fewer hyperparameter trials compared to the revisited study (Akacik & Hoogendoorn, 2025). Notably, TSF-origin models (DLinear, LightTS, MTS-Mixer, FEDformer, ETSformer, Crossformer, PatchTST, and iTransformer) improved by over 3%p, suggesting that their methodologies can be reconsidered for TSC.

5.2 Model Ablation

Table 1: Model ablation for four hypotheses (H1–H4). The best and the second-best are highlighted in bold and underline, respectively.

Model	**(H1)** **kernel size** ✓: $k = 0.02L$ ✗: $k = 3$	**(H2)** **modular SSM** ✓: modular TV/TI ✗: TV only	**(H3)** **skip connection** ✓: not use $\boldsymbol{D}$ ✗: use $\boldsymbol{D}$	**(H4)** **aggregation** ✓: adaptive pool ✗: the others	avg. acc (10)	avg. acc	avg. rank	# win /draw	# lose /draw	rank test
MambaSL	✓	✓	✓	✓	**78.779**	79.802	**2.43**			
w/o H1	✗	✓	✓	✓	77.413	**80.215**	2.53	25	22	0.217
w/o H2	✓	✗	✓	✓	75.659	77.075	5.93	30	5	0.000
w/o H3	✓	✓	✗	✓	77.715	79.163	3.50	22	14	0.071
w/o H4	✓	✓	✓	✗ (fully conn)	76.438	77.722	4.87	24	10	0.003
	✓	✓	✓	✗ (avg pool)	76.900	78.610	3.60	22	15	0.044
	✓	✓	✓	✗ (max pool)	76.448	78.535	3.90	22	12	0.004
	✓	✓	✓	✗ (last step)	75.856	76.848	4.87	25	9	0.001
only H2	✗	✓	✗	✗ (avg pool)	77.092	77.935		20	13	0.011
Mamba	✗	✗	✗	✗ (fully conn)	73.286	74.243		26	5	0.000

Table 1 summarizes the average classification accuracy of ablated models for each hypothesis (H1–H4), providing a systematic exploration of MambaSL's design space. The full results are included in appendix C.2. MambaSL remained competitive with state-of-the-art baselines, even when excluding H1, H3, or H4 individually. Also, none of the three ablations resulted in a statistically significant gains in the rank test. Motivated by this, we additionally ran an ablation that only applies H2; however, this variant failed to surpass the second-best baseline and showed statistically inferior performance ($p = 0.011$), suggesting that all our four hypotheses contribute positively to performance.

Disabling H1 ($k = 3$) yielded the highest average accuracy, surpassing 80%. Its overall ranking, however, remained second, as the gain was largely driven by marginal accuracy changes in the `AF` and `SWJ` datasets, which both have only 15 test samples. Additionally, on three datasets—`AF`, `ER`, and `PEMS`—where MambaSL was outside the top 10 (appendix C.1), a fully connected layer outperformed other classifiers. This suggests that for fixed-length datasets, fully connected readouts can be competitive as long as overfitting is controlled. Nevertheless, across the full benchmark, our multi-head adaptive pooling consistently performs better with greater generalizability.

5.3 Further analysis

Time variance ablation Table 2 shows the classification accuracy of MambaSL under eight configurations of time variance hyperparameters, θ_Δ, $\theta_{\boldsymbol{B}}$, and $\theta_{\boldsymbol{C}}$.

No single combination is overwhelmingly superior, yet models with the LTI setting (all marked ✗) tend to outperform the fully TV setting (all marked ✓) of selective SSM. This contrasts with the findings of Gu & Dao (2024) in their ablation study, where the fully TV setting was superior for language modeling.

Table 2: Ablation on time variance of Δ, $\boldsymbol{B}$, and $\boldsymbol{C}$. The best and the second-best are highlighted in bold and underline, respectively.

TV-Δ	TV-$\boldsymbol{B}$	TV-$\boldsymbol{C}$	avg. acc (10)	avg. acc	avg. rank
✗	✗	✗	**77.280**	77.400	3.87
✗	✗	✓	76.938	77.102	3.93
✗	✓	✗	76.451	77.042	3.80
✗	✓	✓	76.422	**77.767**	**3.60**
✓	✗	✗	76.253	77.707	3.63
✓	✗	✓	76.299	77.148	3.70
✓	✓	✗	76.309	77.085	3.80
✓	✓	✓	75.938	77.055	4.13

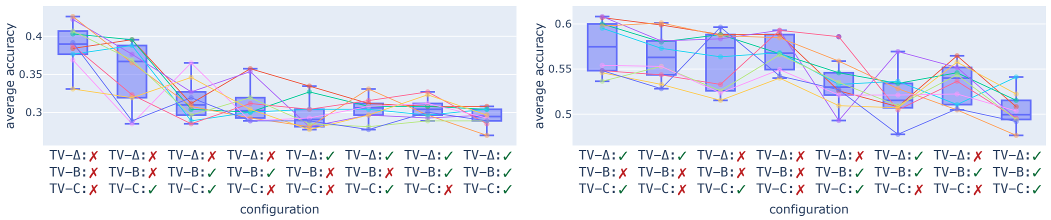

Figure 7: Visualization of classification accuracy of MambaSL along TI/TV configurations on (left) `EC` and (right) `HW` datasets, in order of maximum accuracy.

In some datasets, the trend is particularly clear. As shown on the left side of Figure 7, in `EC`, accuracy increases as more parameters are set to be time-invariant, with Δ having the largest impact. This indicates that dynamic warping of the sampling intervals can distort the chemical reaction signal of ethanol, which can impair classification performance. Furthermore, similar to the right of Figure 7, using TI-$\boldsymbol{B}$ consistently yields better results than using TV-$\boldsymbol{B}$ across many datasets (`HW`, `HB`, `CT`, `DDG`, `UW`, and `RS`), while the opposite trend is also observed (`PEMS`, `CR`, `PD`, and `PS`). By contrast, no dataset exhibits a consistent preference with respect to $\boldsymbol{C}$. These observations support our hypothesis that while the time variance of Δ and $\boldsymbol{B}$ can be dataset-specific, that of $\boldsymbol{C}$ has limited impact, as output-channel mixing naturally occurs in the classifier. The visualizations for all 30 datasets are provided in appendix C.4.

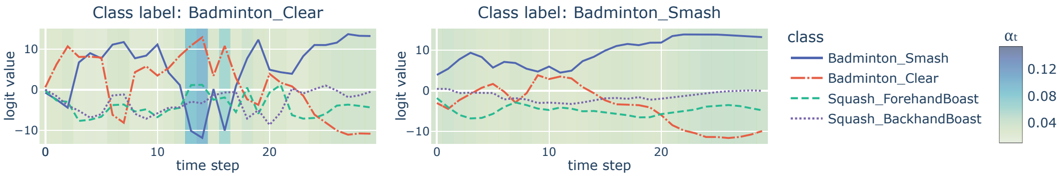

Figure 8: Visualization of adaptive pooling on the `RS` dataset for two samples. Line plots show per-timestep logits $\boldsymbol{l}_t$, and heatmaps illustrate the corresponding per-timestep weights a_t.

Analysis of pooling behavior To further examine the role of adaptive pooling, we analyzed the `RS` dataset, which contains relatively few classes and yields strong performance under max pooling. The left plot in Figure 8 depicts a sample where the predicted label differs between a simple average of per-timestep logits and the weighted average using a_t. As shown, large logit values do not necessarily correspond to large weights, and regions with high weights are often localized. As in the right plot of Figure 8, there are also samples with nearly uniform weights, effectively reducing adaptive pooling to average pooling. This adaptive weighting enables MambaSL to outperform average pooling, achieving the second-highest accuracy on the `RS` dataset (appendices C.1 and C.2).

Effect of model depth Although our main architecture uses a single Mamba block as shown in Figure 2, we also ablated the number of stacked blocks to examine whether a deeper MambaSL further improves performance. Table 3 compares variants with 1, 2, and 3 Mamba blocks under the same training protocol (full results are provided in appendix C.5). We observed that a single layer achieved the best average accuracy and the best average rank across the 30 UEA datasets. While performance gradually decreases as the number of layers increases, the differences are small, and all three variants perform similarly overall. Given these results, we conclude that a carefully configured *single-layer* Mamba is sufficient as a backbone for TSC in this regime, and we adopt the 1-layer MambaSL as our default architecture for both simplicity and efficiency.

Table 3: Classification accuracy (%) of MambaSL according to its model depth. The best and the second-best are highlighted in bold and underline, respectively.

depth	avg. acc (10)	avg. acc	avg. rank (10)	avg. rank	# of win/draw	# of lose/draw	rank test
1	78.827	**79.819**	**1.30**	**1.33**			
2	78.853	79.316	1.90	1.80	26	15	0.035
3	**78.918**	79.279	2.10	2.07	24	12	0.004

5.4 Additional experiments

UEA benchmark classification considering data leakage issue To account for the data-leakage issue reported for `TSLib` in TSC settings (Akacik & Hoogendoorn, 2025; Talukder et al., 2024), we additionally trained MambaSL under the InceptionTime protocol (Ismail Fawaz et al., 2020), where the checkpoint with the lowest training loss is used for evaluation. For comparison, we selected the top three high-performing models from each source—HC2 (Middlehurst et al., 2021), BORF (Spinnato et al., 2024), and our own experiments—to form a comparable set of classical baselines. These results, along with the corresponding evaluation tables, are provided in appendix C.6. While MambaSL shows lower accuracy under the stricter InceptionTime protocol than under the default `TSLib` setting, it remains competitive relative to the strongest non-DL baselines reported in previous studies and in our re-evaluation.

Classification on recent domain-specific dataset Although the UEA archive (Bagnall et al., 2018) covers a broad range of TSC datasets, it does not include more recently released real-world benchmarks. Therefore, we additionally evaluated MambaSL on ADFTD (Miltiadous et al., 2023) and FLAAP (Kumar & Suresh, 2022), two of the most recent datasets benchmarked by Medformer (Wang et al., 2024a) in the medical and human activity recognition (HAR) domains, respectively. Classification results compared with strong baselines in Medformer are provided in appendix C.7. Across both datasets, MambaSL achieves competitive performance without any domain-specific modifications, demonstrating its generalizability to recent TSC tasks.

6 Conclusion

In this study, we introduce four hypotheses as to why Mamba has remained underexplored in TSC despite its success in other sequence domains. With minimal architectural modifications, our *single-layer Mamba* framework, MambaSL, achieved state-of-the-art performance across the entire UEA benchmark. By re-examining 20 prior baselines, we further highlighted systematic differences across backbone structures and demonstrated that Mamba can serve as a strong multivariate TSC backbone.

Nevertheless, our work has two main limitations. First, while our model is robust across the UEA benchmark, it rarely achieves overwhelming superiority on individual datasets, implying that practical use may require domain-specific adaptations. For instance, prior knowledge of input embedding may constrain kernel size, making receptive-field scaling with sequence length suboptimal in certain domains. Second, our study is limited to the first version of Mamba (Gu & Dao, 2024). While Mamba-2 (Dao & Gu, 2024) introduces an efficient parallel Mamba block, applying time-variance modularization requires low-level optimizations beyond the scope of this study.

Overall, our findings demonstrate that a carefully configured single-layer Mamba can serve as a competitive backbone for TSC. Beyond TSC, future work may further improve Mamba by leveraging receptive-field scaling and time-variance control, along with shallow, task-aligned architectural choices and adaptive aggregation strategies.

REPRODUCIBILITY STATEMENT

Source code and scripts are publicly available at GitHub repository , and datasets, along with the best-performing model checkpoints, have been uploaded to Google Drive.

- The source code offers a complete implementation of Mamba and all other baselines, with the exception of dataset and checkpoint downloads. The repository includes grid search script generation, local training execution, pretrained model evaluation, and result visualization.
- Full training logs, corresponding to the grid search results reported in Figure 4 and Table 1, are also provided in the repository. We are confident that the experimental setup and hyperparameter settings mentioned in appendices A and B are identical to the scripts and logs inside the repository.
- The dataset folder also contains preprocessed CWT and ROCKET features for TSCMamba, compatible with the released checkpoints.
- Detailed reproduction instructions are available in the `README.md` file.

THE USE OF LARGE LANGUAGE MODELS

The authors acknowledge the use of ChatGPT-5 and Google Translate only during the writing process to ensure rigorous and concise academic English writing.

REFERENCES

Md Atik Ahamed and Qiang Cheng. TimeMachine: A time series is worth 4 mambas for long-term forecasting. In *ECAI 2024: 27th European Conference on Artificial Intelligence*, volume 392, pp. 1688–1965, 2024.

Md Atik Ahamed and Qiang Cheng. TSCMamba: Mamba meets multi-view learning for time series classification. *Information Fusion*, 120:103079, 2025.

Önder Akacik and Mark Hoogendoorn. ModernTCN revisited: A critical look at the experimental setup in general time series analysis. *Transactions on Machine Learning Research*, 2025. ISSN 2835-8856.

Anthony Bagnall, Hoang Anh Dau, Jason Lines, Michael Flynn, James Large, Aaron Bostrom, Paul Southam, and Eamonn Keogh. The UEA multivariate time series classification archive, 2018, 2018. URL https://arxiv.org/abs/1811.00075.

Dzmitry Bahdanau, Kyunghyun Cho, and Yoshua Bengio. Neural machine translation by jointly learning to align and translate, 2016. URL https://arxiv.org/abs/1409.0473. Accepted at ICLR 2015 as oral presentation.

Shaojie Bai, J. Zico Kolter, and Vladlen Koltun. An empirical evaluation of generic convolutional and recurrent networks for sequence modeling, 2018. URL https://arxiv.org/abs/1803.01271.

Donald J Berndt and James Clifford. Using dynamic time warping to find patterns in time series. In *Proceedings of the 3rd International Conference on Knowledge Discovery and Data Mining*, pp. 359–370, 1994.

Yanping Chen, Eamonn Keogh, Bing Hu, Nurjahan Begum, Anthony Bagnall, Abdullah Mueen, and Gustavo Batista. The UCR time series classification archive, July 2015. www.cs.ucr.edu/~eamonn/time_series_data/.

Tri Dao and Albert Gu. Transformers are SSMs: Generalized models and efficient algorithms through structured state space duality. In *Proceedings of the 41st International Conference on Machine Learning*, volume 235, pp. 10041–10071, 2024.

Angus Dempster, François Petitjean, and Geoffrey I Webb. ROCKET: Exceptionally fast and accurate time series classification using random convolutional kernels. *Data Mining and Knowledge Discovery*, 34(5):1454–1495, 2020.

Angus Dempster, Daniel F. Schmidt, and Geoffrey I. Webb. Minirocket: A very fast (almost) deterministic transform for time series classification. In *Proceedings of the 27th ACM SIGKDD conference on knowledge discovery & data mining*, pp. 248–257, 2021.

Angus Dempster, Daniel F Schmidt, and Geoffrey I Webb. Hydra: Competing convolutional kernels for fast and accurate time series classification. *Data Mining and Knowledge Discovery*, 37:1779–1805, 2023.

Emadeldeen Eldele, Mohamed Ragab, Zhenghua Chen, Min Wu, and Xiaoli Li. TSLANet: Rethinking Transformers for time series representation learning. In *Proceedings of the 41st International Conference on Machine Learning*, volume 235, pp. 12409–12428, 2024.

Albert Gu and Tri Dao. Mamba: Linear-time sequence modeling with selective state spaces. In *The First Conference on Language Modeling*, 2024.

Albert Gu, Isys Johnson, Karan Goel, Khaled Saab, Tri Dao, Atri Rudra, and Christopher Ré. Combining recurrent, convolutional, and continuous-time models with linear state space layers. In *Advances in Neural Information Processing Systems*, pp. 572–585, 2021.

Albert Gu, Karan Goel, and Christopher Re. Efficiently modeling long sequences with structured state spaces. In *International Conference on Learning Representations*, 2022.

Kaiming He, Xiangyu Zhang, Shaoqing Ren, and Jian Sun. Deep residual learning for image recognition. In *Proceedings of the IEEE conference on computer vision and pattern recognition*, pp. 770–778, 2016.

Weizhe Hua, Zihang Dai, Hanxiao Liu, and Quoc Le. Transformer quality in linear time. In *Proceedings of the 39th International Conference on Machine Learning*, volume 162, pp. 9099–9117, 2022.

Hassan Ismail Fawaz, Benjamin Lucas, Germain Forestier, Charlotte Pelletier, Daniel F Schmidt, Jonathan Weber, Geoffrey I Webb, Lhassane Idoumghar, Pierre-Alain Muller, and François Petitjean. InceptionTime: Finding alexnet for time series classification. *Data Mining and Knowledge Discovery*, 34(6):1936–1962, 2020.

Jaeyoung Kim, Mostafa El-Khamy, and Jungwon Lee. Residual LSTM: Design of a deep recurrent architecture for distant speech recognition. In *Interspeech 2017*, pp. 1591–1595, 2017.

Nikita Kitaev, Lukasz Kaiser, and Anselm Levskaya. Reformer: The efficient transformer. In *International Conference on Learning Representations*, 2020.

Prabhat Kumar and S. Suresh. FLAAP: An open human activity recognition (HAR) dataset for learning and finding the associated activity patterns. *Procedia Computer Science*, 212:64–73, 2022.

Barak Lenz, Opher Lieber, Alan Arazi, Amir Bergman, Avshalom Manevich, Barak Peleg, Ben Aviram, Chen Almagor, Clara Fridman, Dan Padnos, Daniel Gissin, Daniel Jannai, Dor Muhlgay, Dor Zimberg, Edden M. Gerber, Elad Dolev, Eran Krakovsky, Erez Safahi, Erez Schwartz, Gal Cohen, Gal Shachaf, Haim Rozenblum, Hofit Bata, Ido Blass, Inbal Magar, Itay Dalmedigos, Jhonathan Osin, Julie Fadlon, Maria Rozman, Matan Danos, Michael Gokhman, Mor Zusman, Naama Gidron, Nir Ratner, Noam Gat, Noam Rozen, Oded Fried, Ohad Leshno, Omer Antverg, Omri Abend, Or Dagan, Orit Cohavi, Raz Alon, Ro'i Belson, Roi Cohen, Rom Gilad, Roman Glozman, Shahar Lev, Shai Shalev-Shwartz, Shaked Haim Meirom, Tal Delbari, Tal Ness, Tomer Asida, Tom Ben Gal, Tom Braude, Uriya Pumerantz, Josh Cohen, Yonatan Belinkov, Yuval Globerson, Yuval Peleg Levy, and Yoav Shoham. Jamba: Hybrid transformer-mamba language models. In *The Thirteenth International Conference on Learning Representations*, 2025.

Kunchang Li, Xinhao Li, Yi Wang, Yinan He, Yali Wang, Limin Wang, and Yu Qiao. VideoMamba: State space model for efficient video understanding. In *Computer Vision – ECCV 2024: 18th European Conference, Milan, Italy, September 29–October 4, 2024, Proceedings, Part XXVI*, pp. 237–255, 2024.

Zhe Li, Zhongwen Rao, Lujia Pan, and Zenglin Xu. MTS-Mixer: Multivariate time series forecasting via factorized temporal and channel mixing, 2023. URL https://arxiv.org/abs/2302.04501.

Liyuan Liu, Haoming Jiang, Pengcheng He, Weizhu Chen, Xiaodong Liu, Jianfeng Gao, and Jiawei Han. On the variance of the adaptive learning rate and beyond. In *International Conference on Learning Representations*, 2020.

Yong Liu, Tengge Hu, Haoran Zhang, Haixu Wu, Shiyu Wang, Lintao Ma, and Mingsheng Long. iTransformer: Inverted Transformers are effective for time series forecasting. In *The Twelfth International Conference on Learning Representations*, 2024.

Donghao Luo and Xue Wang. ModernTCN: A modern pure convolution structure for general time series analysis. In *The Twelfth International Conference on Learning Representations*, 2024.

Stéphane Mallat. *A wavelet tour of signal processing*. Elsevier, 1999.

Leland McInnes, John Healy, and James Melville. UMAP: Uniform manifold approximation and projection for dimension reduction, 2020. URL https://arxiv.org/abs/1802.03426.

Harsh Mehta, Ankit Gupta, Ashok Cutkosky, and Behnam Neyshabur. Long range language modeling via gated state spaces. In *The Eleventh International Conference on Learning Representations*, 2023a.

Harsh Mehta, Ankit Gupta, Ashok Cutkosky, and Behnam Neyshabur. Long range language modeling via gated state spaces. In *The Eleventh International Conference on Learning Representations*, 2023b.

Matthew Middlehurst, James Large, and Anthony Bagnall. The canonical interval forest (cif) classifier for time series classification. In *2020 IEEE international conference on big data (big data)*, pp. 188–195. IEEE, 2020.

Matthew Middlehurst, James Large, and Anthony Bagnall. HIVE-COTE 2.0: a new meta ensemble for time series classification. *Machine Learning*, 110:3211–3243, 2021.

Matthew Middlehurst, Ali Ismail-Fawaz, Antoine Guillaume, Christopher Holder, David Guijo-Rubio, Guzal Bulatova, Leonidas Tsaprounis, Lukasz Mentel, Martin Walter, Patrick Schäfer, et al. aeon: a python toolkit for learning from time series. *Journal of Machine Learning Research*, 25(289):1–10, 2024.

Andreas Miltiadous, Katerina D Tzimourta, Theodora Afrantou, Panagiotis Ioannidis, Nikolaos Grigoriadis, Dimitrios G Tsalikakis, Pantelis Angelidis, Markos G Tsipouras, Euripidis Glavas, Nikolaos Giannakeas, et al. A dataset of scalp EEG recordings of alzheimer's disease, frontotemporal dementia and healthy subjects from routine EEG. *Data*, 8(6):95, 2023.

Yuqi Nie, Nam H. Nguyen, Phanwadee Sinthong, and Jayant Kalagnanam. A time series is worth 64 words: Long-term forecasting with Transformers. In *The Eleventh International Conference on Learning Representations*, 2023.

John Paparrizos and Luis Gravano. k-Shape: Efficient and accurate clustering of time series. In *Proceedings of the 2015 ACM SIGMOD International Conference on Management of Data*, pp. 1855–1870, 2015.

Francesco Spinnato, Riccardo Guidotti, Anna Monreale, and Mirco Nanni. Fast, interpretable and deterministic time series classification with a bag-of-receptive-fields. *IEEE Access*, 2024.

state-spaces. mamba. https://github.com/state-spaces/mamba, 2025. Accessed: 8 August 2025.

Sabera J Talukder, Yisong Yue, and Georgia Gkioxari. TOTEM: TOkenized time series EMbeddings for general time series analysis. *Transactions on Machine Learning Research*, 2024. ISSN 2835-8856.

Chang Wei Tan, Angus Dempster, Christoph Bergmeir, and Geoffrey I Webb. MultiRocket: multiple pooling operators and transformations for fast and effective time series classification. *Data Mining and Knowledge Discovery*, 36:1623–1646, 2022.

Ashish Vaswani, Noam Shazeer, Niki Parmar, Jakob Uszkoreit, Llion Jones, Aidan N Gomez, Łukasz Kaiser, and Illia Polosukhin. Attention is all you need. In *Advances in Neural Information Processing Systems*, 2017.

Shiyu Wang, Jiawei LI, Xiaoming Shi, Zhou Ye, Baichuan Mo, Wenze Lin, Ju Shengtong, Zhixuan Chu, and Ming Jin. TimeMixer++: A general time series pattern machine for universal predictive analysis. In *The Thirteenth International Conference on Learning Representations*, 2025a.

Yihe Wang, Nan Huang, Taida Li, Yujun Yan, and Xiang Zhang. Medformer: A multi-granularity patching transformer for medical time-series classification. In *Advances in Neural Information Processing Systems*, volume 37, pp. 36314–36341, 2024a.

Yuxuan Wang, Haixu Wu, Jiaxiang Dong, Yong Liu, Mingsheng Long, and Jianmin Wang. Deep time series models: A comprehensive survey and benchmark, 2024b. URL `https://arxiv.org/abs/2407.13278`.

Zihan Wang, Fanheng Kong, Shi Feng, Ming Wang, Xiaocui Yang, Han Zhao, Daling Wang, and Yifei Zhang. Is Mamba effective for time series forecasting? *Neurocomputing*, 619:129178, 2025b.

Yunshi Wen, Tengfei Ma, Ronny Luss, Debarun Bhattacharjya, Achille Fokoue, and Anak Agung Julius. Shedding light on time series classification using interpretability gated networks. In *The Thirteenth International Conference on Learning Representations*, 2025.

Frank Wilcoxon. Individual comparisons by ranking methods. *Biometrics bulletin*, 1(6):80–83, 1945.

Gerald Woo, Chenghao Liu, Doyen Sahoo, Akshat Kumar, and Steven Hoi. ETSformer: Exponential smoothing Transformers for time-series forecasting, 2022. URL `https://arxiv.org/abs/2202.01381`.

Haixu Wu, Tengge Hu, Yong Liu, Hang Zhou, Jianmin Wang, and Mingsheng Long. TimesNet: Temporal 2d-variation modeling for general time series analysis. In *The Eleventh International Conference on Learning Representations*, 2023.

Zhihan Yue, Yujing Wang, Juanyong Duan, Tianmeng Yang, Congrui Huang, Yunhai Tong, and Bixiong Xu. TS2Vec: Towards universal representation of time series. In *Proceedings of the AAAI Conference on Artificial Intelligence*, volume 36, pp. 8980–8987, 2022.

Ailing Zeng, Muxi Chen, Lei Zhang, and Qiang Xu. Are Transformers effective for time series forecasting? In *Proceedings of the AAAI Conference on Artificial Intelligence*, volume 37, pp. 11121–11128, 2023.

T Zhang, Y Zhang, W Cao, J Bian, X Yi, S Zheng, and J Li. Less Is More: Fast multivariate time series forecasting with light sampling-oriented MLP structures, 2022. URL `https://arxiv.org/abs/2207.01186`.

Yunhao Zhang and Junchi Yan. Crossformer: Transformer utilizing cross-dimension dependency for multivariate time series forecasting. In *The Eleventh International Conference on Learning Representations*, 2023.

Tian Zhou, Ziqing Ma, Qingsong Wen, Xue Wang, Liang Sun, and Rong Jin. FEDformer: Frequency enhanced decomposed Transformer for long-term series forecasting. In *Proceedings of the 39th International Conference on Machine Learning*, volume 162, pp. 27268–27286, 2022.

Tian Zhou, Peisong Niu, Xue Wang, Liang Sun, and Rong Jin. One Fits All: Power general time series analysis by pretrained LM. In *Advances in Neural Information Processing Systems*, volume 36, pp. 43322–43355, 2023.

A EXPERIMENTAL SETUP

Environment All experiments were implemented in Python 3.12.8 and PyTorch 2.5.1. Most were run on NVIDIA GTX 1080 Ti (11GB), while a few required NVIDIA A100 (40GB) on Google Colab due to memory limits. Classical baselines used the `aeon` toolkit (Middlehurst et al., 2024), and all deep models except TSLANet were integrated into the Time-Series Library (`TSLib`) (Wu et al., 2023; Wang et al., 2024b). For models supported in `TSLib`, we used the provided code; for others, we adapted the authors' official implementations. All source code is available in our GitHub repository (see reproducibility statement).

Dataset The UEA archive (Bagnall et al., 2018) provides 30 multivariate TSC datasets with diverse sample sizes, input dimensions, lengths, and class counts (Table 4). As `TSLib` has become a widely used framework, a subset of 10 datasets (`EC`, `FD`, `HW`, `HB`, `JV`, `PEMS`, `SRS1`, `SRS2`, `SAD`, and `UW`) is commonly used in recent TSC benchmarking practices.

Table 4: Summary of the 30 UEA datasets used in our experiments

Dataset	Code	Train Size	Test Size	Length	Variables	Classes
EthanolConcentration	`EC`	261	263	1751	3	4
FaceDetection	`FD`	5890	3524	62	144	2
Handwriting	`HW`	150	850	152	3	26
Heartbeat	`HB`	204	205	405	61	2
JapaneseVowels	`JV`	270	370	7–29	12	9
PEMS-SF	`PEMS`	267	173	144	963	7
SelfRegulationSCP1	`SRS1`	268	293	896	6	2
SelfRegulationSCP2	`SRS2`	200	180	1152	7	2
SpokenArabicDigits	`SAD`	6599	2199	4–93	13	10
UWaveGestureLibrary	`UW`	120	320	315	3	8
ArticularyWordRecognition	`AWR`	275	300	144	9	25
AtrialFibrillation	`AF`	15	15	640	2	3
BasicMotions	`BM`	40	40	100	6	4
CharacterTrajectories	`CT`	1422	1436	60–182	3	20
Cricket	`CR`	108	72	1197	6	12
DuckDuckGeese	`DDG`	50	50	270	1345	5
EigenWorms	`EW`	128	131	17984	6	5
Epilepsy	`EP`	137	138	206	3	4
ERing	`ER`	30	270	65	4	6
FingerMovements	`FM`	316	100	50	28	2
HandMovementDirection	`HMD`	160	74	400	10	4
InsectWingbeat	`IW`	25000	25000	2–22	200	10
Libras	`LIB`	180	180	45	2	15
LSST	`LSST`	2459	2466	36	6	14
MotorImagery	`MI`	278	100	3000	64	2
NATOPS	`NATO`	180	180	51	24	6
PenDigits	`PD`	7494	3498	8	2	10
PhonemeSpectra	`PS`	3315	3353	217	11	39
RacketSports	`RS`	151	152	30	6	4
StandWalkJump	`SWJ`	12	15	2500	4	3

Metrics The evaluation metrics reported in our figures and tables are summarized as follows:

- **avg. acc:** Average accuracy (%) across all UEA datasets.
- **avg. acc (10):** Average accuracy (%) for 10 UEA datasets, following prior TSC practices.
- **avg. rank:** Average rank of each model across all UEA datasets.
- **# of top-N:** Count of datasets in which each model is in top-N.
- **# of win/draw:** Count of datasets where proposed model achieved higher or the same accuracy.
- **# of loss/draw:** Count of datasets where proposed model achieved lower or the same accuracy.
- **rank test:** p-value of Wilcoxon signed-rank test (Wilcoxon, 1945). A value smaller than the significance level (0.05) indicates that proposed model ranked greater than the selected.

B Hyperparameter settings

B.1 Basic hyperparameter settings

We standardized experimental hyperparameter settings across all models to focus on model tuning, where most were chosen as common values across prior UEA benchmarks and `TSLib`:

- **Batch size**: 16 (some experiments used smaller batch size as described in appendix C.1.)
- **Learning rate**: 0.001
- **Learning rate scheduler**: none
- **Optimizer**: RAdam (Liu et al., 2020)
- **Train epochs**: 100
- **Patience**: 10
- **Dropout**: 0.1
- **Seed**: 2021 (for DL models)

Although this unified setting may deviate from model-specific defaults, extensive model-level grid searches compensated for potential performance degradation (see appendix C.3).

B.2 Model hyperparameter settings for grid search

We primarily considered the hyperparameter settings that were tested in either the original papers or the source code scripts, and we also referred to the hyperparameters that were set in `TSLib` scripts. For TSF-origin and foundation models that do not provide classification scripts, we tend to choose the same or smaller values than in forecasting scripts since we empirically found that many UEA datasets require compact model sizes compared to TSF datasets. Over 200 candidate settings were evaluated per model–dataset pair, except for some models that did not require significant extension. The hyperparameters explored are as below:

- **Non-DL**
  - DTW$_D$: fixed implementations (no learnable hyperparameters).
  - ROCKET, HC2, Hydra, MR+Hydra: 3 combinations
    - `seed`: 0, 1, 2
    - Other parameters are fixed to the default optimal setting of the original papers since the models themselves have either large number (1e-4) of kernels or ensemble mechanism.

- **MLP-based models**
  - DLinear: 15 combinations
    - `moving_avg`: 0.5%, 1%, 2%, 3%, 4%, 5%, 10%, 15%, 20%, 25%, 30%, 35%, 40%, 45%, 50% of sequence length
    - Since DLinear only has one model parameter to be tuned, we didn't over-expand the number of hyperparameter combinations beyond 200.
  - LightTS: 100 combinations
    - `d_model`: 32, 64, 128, 256, 512
    - `chunk_size`: 1/21 – 1/2 of sequence length
    - Since LightTS only has two model parameters to be tuned, we didn't over-expand the number of hyperparameter combinations beyond 200.
  - MTS-Mixer: 256 combinations
    - `e_layers`: 2
    - `d_model`: 128, 256, 512, 1024
    - `d_ff`: 0, 2, 4, 8, 16, 32, 64, 128
    - `fac_C`: 0 (False) if `d_ff` is 0, else 1 (True)
    - `down_sampling_window`: 0, 1%, 2%, 3%, 5%, 7.5%, 10%, 12.5% of sequence length
    - `fac_T`: 0 (False) if `down_sampling_window` is 0, else 1 (True)
    - `use_norm`: 1 (True)

- **CNN-based models**
  - TimesNet: 252 combinations
    - `e_layers`: 2, 3, 4
    - `(d_model, d_ff)`: (8,16), (8,32), (8,64), (16,16), (16,32), (16,64), (32,32), (32,64), (32,128), (64,64), (64,128), (64,256), (128,128), (128,256)
    - `top_k`: 1, 2, 3
    - `num_kernels`: 4, 6
  - ModernTCN: 252 combinations
    - `ffn_ratio`: 1, 2, 4
    - `patch_size`: 2.5%, 5%, 7.5%, 10%, 15%, 20%, 25% of sequence length
    - `patch_stride`: 50% of `patch_size`
    - `(num_blocks, large_size, small_size, dims)`: (“1”, “13”, “5”, “32”), (“1”, “13”, “5”, “64”), (“1”, “13”, “5”, “128”), (“1”, “13”, “5”, “256”), (“1 1”, “9 9”, “5 5”, “32 64”), (“1 1”, “9 9”, “5 5”, “64 128”), (“1 1”, “9 9”, “5 5”, “128 256”), (“1 1”, “13 13”, “5 5”, “32 64”), (“1 1”, “13 13”, “5 5”, “64 128”), (“1 1”, “13 13”, “5 5”, “128 256”), (“1 1 1”, “9 9 9”, “5 5 5”, “32 64 128”), (“1 1 1”, “13 13 13”, “5 5 5”, “32 64 128”)
  - TSLANet: 252 combinations
    - `depth`: 1, 2, 3
    - `emb_dim`: 32, 64, 128, 256
    - `mlp_ratio`: 1, 2, 3
    - `patch_size`: 2.5%, 5%, 7.5%, 10%, 15%, 20%, 25% of sequence length
    - `patch_stride`: 50% of `patch_size`
    - `masking_ratio`: 0.4
    - `ICB`: 1 (True)
    - `ASB`: 1 (True)
    - `adaptive_filter`: 1 (True)
    - `load_from_pretrained`: 1 (True)
    - `pretrain_lr`: 0.001
    - `pretrain_epoch`: 50
  - TimeMixer++: 216 combinations
    - `down_sampling_method`: “conv”
    - `down_sampling_layers`: 1, 2, 3
    - `down_sampling_window`: 2
    - `num_kernels`: 6
    - `e_layers`: 1, 2, 3, 4
    - `d_model`: 16, 32, 64
    - `d_ff`: 16, 32, 64
    - `n_heads`: 8
    - `top_k`: 2, 3

- **Transformer-based models**
  - FEDformer: 250 combinations
    - `moving_avg`: 0.5%, 1%, 2%, 3%, 5%, 10%, 20%, 30%, 40%, 50% of sequence length
    - `e_layers`: 2
    - `d_model`: 32, 64, 128, 256, 512
    - `d_ff`: 128, 256, 512, 1024, 2048
    - `n_heads`: 8
  - ETSformer: 240 combinations
    - `e_layers`: 1, 2
    - `d_model`: 32, 64, 128, 256, 512
    - `d_ff`: 64, 128, 256, 512, 1024, 2048
    - `n_heads`: 8
    - `top_k`: 1, 2, 3, 4
  - Crossformer: 288 combinations
    - `e_layers`: 1, 2, 3
    - `d_model`: 32, 64, 128, 256
    - `d_ff`: 64, 128, 256, 512
    - `n_heads`: 4
    - `factor`: 3, 10
    - `seg_len`: 6, 12, 24 (change the code of `TSLib` to modify the fixed value)
  - PatchTST: 252 combinations
    - `e_layers`: 1, 2, 3
    - `d_model`: 16, 32, 64, 128
    - `d_ff`: 64, 128, 256
    - `n_heads`: 4 if `d_model` $\in \{16, 32\}$ else 16
    - `patch_size`: 2.5%, 5%, 7.5%, 10%, 15%, 20%, 25% of sequence length
    - `patch_stride`: 50% of `patch_size`
  - GPT4TS: 252 combinations
    - `e_layers`: 3, 4, 5, 6
    - `d_model`: 768 (fixed since the model use pretrained GPT-2)
    - `d_ff`: 768 (fixed since the model use pretrained GPT-2)
    - `patch_size`: 1/25 – 1/5 of sequence length
    - `patch_stride`: 25%, 50%, 100% of `patch_size`
  - iTransformer: 240 combinations
    - `e_layers`: 1, 2, 3, 4
    - `d_model`: 64, 128, 256, 512, 1024, 2048
    - `d_ff`: 64, 128, 256, 512, 1024
    - `n_heads`: 8
    - `factor`: 1, 3

- **Shape-based model**
  - InterpGN: 243 combinations
    - `dnn_type`: “FCN”
    - `num_shaplet`: 5, 10, 15
    - `lambda_div`: 0, 0.1, 1.0
    - `lambda_reg`: 0, 0.1, 1.0
    - `epsilon`: 0.5, 1.0, 2.0
    - `gating_value`: 0.5, 0.75, 1.0
    - `distance_func`: “euclidean”
    - `memory_efficient`: False
    - `sbm_cls`: “linear”

- **Mamba-based models**
  - TSCMamba: 288 combinations
    - `d_model`: 64, 128, 256
    - `e_layers`: 1, 2
    - `expand`: 1, 2
    - `d_conv`: 2, 4
    - `d_ff` (`d_state`): 32, 64, 128
    - `no_rocket`: 0 (False)
    - `half_rocket`: 0 (False), 1 (True)
    - `additive_fusion`: 0 (multiplicative fusion), 1 (additive fusion)
    - `max_pooling`: 0 (avg pooling), 1 (max pooling)
    - `channel_token_mixing`: 0 (False)
    - `only_forward_scan`: 0 (False)
    - `flip_dir`: 2 (vertical flip)
    - `reverse_flip`: 0 (False)
    - `patch_size`: 8
    - `patch_stride`: 8
    - `rescale_size`: 64
    - `variation`: 64
    - `initial_focus`: 1.0
  - MambaSL (ours): 240 combinations
    - `d_model` (d_m): 32, 64, 128, 256, 512, 1024
    - `d_ff` (d_s): 1, 2, 4, 8, 16
    - `tv_dt` (θ_Δ): 0 (False), 1 (True)
    - `tv_B` ($\theta_{\boldsymbol{B}}$): 0 (False), 1 (True)
    - `tv_C` ($\theta_{\boldsymbol{C}}$): 0 (False), 1 (True)
    - `use_D`: 0 (False)
    - `expand`: 1
    - `d_conv`: 4

C Additional Experimental Results

C.1 Full results of TSC models on the UEA benchmark

Table 5 presents the full experimental results corresponding to Figure 4. As mentioned in appendix A, some experiments could not be run on the GTX 1080 Ti GPU with batch size 16. Footnotes in the table indicate such experiments. We only used the A100 GPU for cases that could not be run on the 1080 Ti with batch size 4. Also, note that only one hyperparameter combination was tested in our limited resource environment for TSCMamba (Ahamed & Cheng, 2025)–`IW` pair, since preprocessing took over 2 days and training took over 12 hours per epoch.

Table 5: Classification accuracy (%) of TSC models on 30 datasets from the UEA archives. The best and the second-best are highlighted in bold and underline, respectively.

(a) Classification results from DTW$_D$ to ModernTCN.

	non-DL					MLP-based			CNN-based	
	DTW$_D$ (1994)	ROCKET (2020)	HC2 (2021)	Hydra (2023)	MR+ Hydra (2023)	DLinear (2023)	LightTS (2022)	MTS-Mixer (2023)	TimesNet (2023)	Modern TCN (2024)
EC	32.319	44.487	52.852	<u>54.373</u>	**60.076**	31.179	32.319	30.798	33.460	32.319
FD	52.866	61.606	61.379	60.982	61.294	69.495	68.473	68.530	<u>70.148</u>	66.998
HW	60.706	59.294	56.000	56.353	53.529	23.765	25.059	19.647	37.529	30.118
HB	71.707	75.610	78.537	76.585	77.073	76.585	77.561	79.024	**83.902**	78.049
JV	95.946	83.784	98.378	97.838	98.378	96.486	96.757	95.946	98.649	98.649
PEMS	71.098	84.393	<u>97.688</u>	**98.266**	82.659	82.659	87.861	82.081	87.861	86.705^A
SRS1	77.474	85.666	89.078	86.689	**94.881**	92.833	92.833	78.840	92.150	93.515
SRS2	53.889	55.556	54.444	58.889	55.000	57.222	59.444	58.333	60.000	60.000
SAD	97.226	99.227	99.136	99.136	99.045	96.953	98.226	99.454	99.545	99.500
UW	90.313	94.063	94.063	<u>94.375</u>	94.063	82.813	89.063	83.125	88.438	88.438
AWR	98.667	**99.333**	**99.333**	**99.333**	**99.333**	97.667	98.333	<u>99.000</u>	98.667	98.667
AF	20.000	6.667	20.000	26.667	6.667	53.333	<u>73.333</u>	60.000	66.667	<u>73.333</u>
BM	<u>97.500</u>	**100.000**	**100.000**	**100.000**	**100.000**	87.500	**100.000**	**100.000**	**100.000**	**100.000**
CT	98.816	99.304	99.304	99.164	99.373	98.120	98.955	97.981	98.747	99.304
CR	**100.000**	**100.000**	**100.000**	**100.000**	<u>98.611</u>	91.667	93.056	97.222	97.222	97.222
DDG	58.000	52.000	70.000	68.000	60.000	66.000	56.000	68.000^8	68.000	66.000^A
EW	61.832	91.603	<u>97.710</u>	**98.473**	**98.473**	42.748^A	54.198^8	66.412	63.359	64.122
EP	96.377	<u>99.275</u>	**100.000**	**100.000**	**100.000**	65.217	97.101	66.667	96.377	96.377
ER	91.481	<u>98.889</u>	<u>98.889</u>	<u>98.889</u>	**99.259**	91.852	94.444	77.778	95.556	97.407
FM	53.000	57.000	61.000	55.000	60.000	62.000	64.000	63.000	66.000	67.000
HMD	18.919	51.351	48.649	51.351	36.486	66.216	66.216	70.270	**72.973**	66.216
IW	48.692	38.524	66.796	67.052	65.744	18.996	71.676	72.424	64.024	**75.588**
LIB	87.222	90.556	94.444	93.333	93.333	70.556	89.444	34.444	88.333	90.000
LSST	55.109	64.031	<u>66.383</u>	**66.504**	64.274	34.023	41.525	34.185	44.120	43.593
MI	50.000	54.000	50.000	54.000	51.000	64.000	68.000	66.000	68.000	67.000
NATO	88.333	89.444	91.111	90.000	93.333	96.111	97.222	95.000	98.333	95.556
PD	97.713	98.228	97.656	97.856	97.284	92.481	96.998	46.941	98.914	98.513
PS	15.121	27.826	33.015	<u>33.164</u>	**33.642**	6.651	16.224	5.428	14.524	13.749
RS	80.263	90.789	90.132	91.447	90.132	78.947	81.579	86.842	89.474	84.211
SWJ	20.000	46.667	40.000	40.000	66.667	53.333	73.333	66.667	66.667	<u>80.000</u>
avg. acc (10)	70.354	74.368	78.156	<u>78.349</u>	77.600	70.999	72.760	69.578	75.168	73.429
avg. acc	68.020	73.306	76.866	77.124	76.320	68.247	75.308	69.001	76.921	76.938
avg. rank	16.03	11.20	8.90	8.83	9.40	16.80	11.83	13.90	8.67	9.13
# of top-1	1	3	4	<u>7</u>	**8**	0	1	1	3	2
# of top-5	2	10	13	13	12	0	6	3	9	8
# of top-10	5	15	19	17	16	5	11	9	17	16
# of win/draw	29	24	20	20	21	28	25	28	24	24
# of lose/draw	2	9	14	13	11	3	7	4	8	8
rank test	0.000	0.001	0.056	0.034	0.015	0.000	0.000	0.000	0.004	0.001

All experiments were run on 1080 Ti with batch size 16 except below:

[8] The experiments were run with batch size 8

[4] The experiments were run with batch size 4

[A] The experiments were run on A100 GPU

Table 5: *(Continued.)* Classification accuracy (%) of TSC models on 30 datasets from the UEA archives. The best and the second-best are highlighted in bold and underline, respectively.

(b) Classification results from TSLANet to MambaSL. "*" indicates "former" in Transformer-based models.

	CNN-based		Transformer-based						shape-based	Mamba-based	
	TSLANet (2024)	Time Mixer++ (2025a)	FED* (2022)	ETS* (2022)	Cross* (2023)	PatchTST (2023)	GPT4TS (2023)	iTrans* (2024)	InterpGN (2025)	TSC Mamba (2025)	**MambaSL (proposed)**
EC	31.939	34.601	33.840	33.080	43.346	32.700	32.319	31.939	28.897	30.798	42.586
FD	66.969	69.665	69.892	68.331	69.637	68.076	68.615	68.417	63.791	**70.204**	69.296
HW	**62.000**	33.647	33.412	35.647	30.353	29.529	34.118	31.294	58.706	45.059	60.824
HB	79.512	80.488	78.049	78.537	79.024	73.659	79.024	78.049	80.488	78.537	80.488
JV	98.919	99.189	97.568	98.378	98.378	97.027	98.108	98.108	**99.730**	98.378	98.649
PEMS	89.017	89.017	89.017	87.861	89.595[8]	89.017[4]	88.439	91.329[8]	86.127	90.173	85.549
SRS1	89.761	92.150	75.085	92.150	93.857	89.078	93.174	93.857	90.444	92.833	92.491
SRS2	63.889	60.556	59.444	60.000	61.667	61.667	60.556	58.889	58.333	62.222	**65.000**
SAD	98.045	99.545	99.454	99.000	98.863	98.818	99.591	99.318	99.864	95.816	**99.955**
UW	94.375	90.625	79.688	89.688	88.438	89.375	89.063	90.000	88.438	**95.313**	93.438
AWR	**99.333**	99.000	92.333	98.667	98.667	98.667	98.667	99.000	99.000	**99.333**	**99.333**
AF	66.667	66.667	73.333	**80.000**	73.333	**80.000**	66.667	66.667	46.667	66.667	53.333
BM	**100.000**	**100.000**	95.000	**100.000**	**100.000**	85.000	**100.000**	97.500	**100.000**	**100.000**	**100.000**
CT	99.164	99.373	97.284	98.468	98.955	98.398	99.373	98.886	**99.791**	99.513	99.721
CR	91.667	98.611	90.278	98.611	97.222	97.222	97.222	97.222	**100.000**	**100.000**	**100.000**
DDG	74.000	74.000	42.000	42.000	72.000[4]	40.000[4]	66.000	60.000[8]	**76.000**[A]	50.000	70.000
EW	81.679	61.069[A]	63.359[4]	70.992[4]	58.015[4]	57.252	66.412	59.542	82.443[A]	88.550	83.969[4]
EP	**100.000**	94.928	92.754	92.754	95.652	98.551	89.855	80.435	97.826	99.275	97.826
ER	85.926	96.296	95.926	96.296	97.407	96.667	96.296	94.815	87.778	97.037	93.704
FM	68.000	67.000	**72.000**	66.000	64.000	63.000	66.000	64.000	67.000	66.000	71.000
HMD	48.649	**72.973**	71.622	63.514	66.216	63.514	70.270	58.108	45.946	60.811	70.270
IW	10.012	64.192	65.244	64.868	73.712	60.936	61.396	73.436	67.180	68.244[*]	66.304
LIB	95.556	88.333	93.333	90.000	90.556	81.667	87.778	91.667	**97.222**	91.667	91.667
LSST	51.014	44.444	40.998	41.241	41.768	56.732	38.078	40.673	59.570	60.057	45.580
MI	**71.000**	67.000	65.000	67.000[8]	68.000[4]	69.000	67.000	67.000	67.000[A]	67.000	69.000
NATO	**99.444**	96.111	96.111	93.333	93.889	80.556	96.111	88.889	98.889	92.222	98.889
PD	99.028	98.599	98.599	98.542	98.513	98.485	98.513	98.428	**99.342**	98.513	99.257
PS	4.921	15.508	11.691	14.316	14.256	15.091	13.123	11.542	33.075	23.800	30.331
RS	**94.079**	91.447	84.868	85.526	87.500	85.526	86.842	81.579	91.447	90.789	92.763
SWJ	73.333	73.333	66.667	66.667[8]	80.000	**86.667**	73.333	73.333	60.000	73.333	73.333
avg. acc (10)	77.443	74.948	71.545	74.267	75.316	72.895	74.301	74.120	75.482	75.933	**78.827**
avg. acc	76.263	77.279	74.128	75.716	77.427	74.729	76.065	74.797	77.700	78.405	**79.819**
avg. rank	7.80	7.03	12.33	10.63	8.50	12.60	9.50	11.83	7.87	7.10	**5.30**
# of top-1	7	2	1	2	1	2	1	0	7	5	5
# of top-5	16	12	6	2	12	4	6	4	14	12	**18**
# of top-10	21	24	10	13	17	8	18	10	20	25	**27**
# of win/draw	18	23	23	27	21	24	26	25	21	20	
# of lose/draw	15	10	7	4	10	7	7	7	14	15	
rank test	0.029	0.005	0.000	0.000	0.005	0.000	0.000	0.000	0.026	0.039	

All experiments were run on 1080 Ti with batch size 16 except below:

[8] The experiments were run with batch size 8

[4] The experiments were run with batch size 4

[A] The experiments were run on A100 GPU

[*] Little hyperparameter search was performed since it took over two weeks conducting a single experiment.

C.2 Full results of model ablation on the UEA benchmark

Table 6 presents the complete ablation results corresponding to Table 1. For a clear comparison, we also performed the hyperparameter grid search for each ablated model. Model rankings were computed within the ablated variants, while additional experimental results are included for reference.

Since removing H2 reduces the number of valid hyperparameter configurations to one-eighth, we extended the search space of Mamba's hyperparameters (`expand` and `d_conv`) and compared the results. As expected, performance improved with broader exploration, yet the model still underperformed on datasets such as `EC` and `NATO`, where the LTI setting remains advantageous.

Table 6: Classification accuracy (%) of ablated models on all 30 datasets from the UEA archives. `d_model`, `d_state`, `expand`, and `d_conv` are four basic hyperparameters that affect the model capacity of Mamba. The best and the second-best are highlighted in bold and underline, respectively.

	ablation								additional		
	w/o H1	w/o H2	w/o H3	w/o H4				**proposed**	Mamba	w/ H2	w/o H2
kernel size ✓: $k = 0.02L$ ✗: $k = 3$	✗	✓	✓	✓	✓	✓	✓	✓	✗	✗	✓
modular SSM ✓: modular TV/TI ✗: TV only	✓	✗	✓	✓	✓	✓	✓	✓	✗	✓	✗
skip connection ✓: not use D ✗: use D	✓	✓	✗	✓	✓	✓	✓	✓	✗	✗	✓
aggregation ✓: adaptive pool. ✗: the others	✓	✓	✓	✗ (full)	✗ (avg)	✗ (max)	✗ (last)	✓	✗ (full)	✗ (avg)	✓
`d_model`	32..1024	32..1024	32..1024	32..1024	32..1024	32..1024	32..1024	32..1024	32..1024	32..1024	32..1024
`d_state`	1..16	1..16	1..16	1..16	1..16	1..16	1..16	1..16	1..16	1..16	1..16
`expand`	1	1	1	1	1	1	1	1	1	1	*1,2,4*
`d_conv`	4	4	4	4	4	4	4	4	4	4	*1,2,4*
# of exp	240	30	240	240	240	240	240	240	30	240	270
EC	33.080	32.319	39.544	34.601	32.700	41.825	33.080	**42.586**	30.418	34.221	33.460
FD	69.296	68.587	69.211	70.006	**70.034**	69.012	66.827	69.296	68.785	69.154	69.495
HW	60.235	54.000	58.000	47.294	59.882	45.529	56.706	**60.824**	30.941	60.471	56.000
HB	**80.976**	79.024	80.000	80.000	80.488	**80.976**	78.537	80.488	77.073	80.976	80.976
JV	98.649	98.108	98.649	98.649	98.108	**98.919**	**98.919**	98.649	97.297	97.838	98.919
PEMS	85.549	82.659	87.283	**90.751**	82.659	85.549	89.595	85.549	93.064	83.815	85.549
SRS1	92.150	89.761	91.809	**93.174**	91.468	90.102	87.713	92.491	92.833	91.126	91.809
SRS2	61.111	61.111	60.556	61.111	60.000	63.333	61.111	**65.000**	58.889	60.556	62.222
SAD	**99.955**	99.773	99.909	99.727	99.909	99.864	99.818	**99.955**	99.181	99.955	99.818
UW	93.125	91.250	92.188	89.063	**93.750**	89.375	86.250	93.438	84.375	92.813	93.438
AWR	**99.333**	**99.333**	99.000	99.000	**99.333**	99.000	97.000	**99.333**	97.667	99.000	99.333
AF	**73.333**	46.667	53.333	66.667	53.333	66.667	66.667	53.333	66.667	46.667	60.000
BM	**100.000**	**100.000**	**100.000**	**100.000**	**100.000**	**100.000**	**100.000**	**100.000**	97.500	100.000	100.000
CT	99.582	99.443	99.513	99.095	**99.791**	99.234	99.582	99.721	98.816	99.791	99.582
CR	**100.000**	**100.000**	**100.000**	98.611	**100.000**	**100.000**	**100.000**	**100.000**	97.222	100.000	100.000
DDG	70.000	66.000	74.000	64.000	72.000	76.000	**80.000**	70.000	52.000	72.000	74.000
EW	**85.496**	83.206	84.733	67.176	83.969	84.733	51.908	83.969	67.176	75.573	85.496
EP	97.826	97.826	97.101	96.377	97.826	**98.551**	97.826	97.826	92.754	97.101	97.826
ER	93.704	91.852	94.444	**95.926**	95.185	91.852	92.222	93.704	94.444	96.296	94.815
FM	**71.000**	64.000	65.000	69.000	64.000	67.000	68.000	**71.000**	64.000	64.000	68.000
HMD	**72.973**	64.865	68.919	68.919	68.919	56.757	50.000	70.270	52.703	74.324	68.919
IW	66.304	65.952	66.220	65.124	66.084	66.392	**66.584**	66.304	62.684	66.396	66.756
LIB	**91.667**	**91.667**	90.556	86.111	91.111	88.889	88.889	**91.667**	82.778	92.778	92.222
LSST	45.580	43.593	**46.513**	43.390	45.174	43.593	42.701	45.580	37.307	43.917	44.282
MI	65.000	65.000	**70.000**	**70.000**	65.000	66.000	65.000	69.000	65.000	63.000	66.000
NATO	**98.889**	97.222	**98.889**	97.778	**98.889**	**98.889**	**98.889**	**98.889**	95.556	98.333	98.333
PD	99.257	99.142	99.371	99.114	**99.428**	99.085	98.999	99.257	98.799	99.314	99.314
PS	29.615	29.764	30.063	16.880	**31.792**	27.528	27.140	30.331	13.809	31.226	29.764
RS	92.763	90.132	93.421	90.789	90.789	**94.737**	88.816	92.763	84.211	94.079	90.789
SWJ	**80.000**	60.000	66.667	73.333	66.667	66.667	66.667	73.333	73.333	53.333	73.333
avg. acc (10)	77.413	75.659	77.715	76.438	76.900	76.448	75.856	**78.827**	73.286	77.092	77.169
avg. acc	**80.215**	77.075	79.163	77.722	78.610	78.535	76.848	79.819	74.243	77.935	79.348
avg. rank	2.53	5.93	3.53	4.90	3.60	3.90	4.87	**2.40**			
# of win/draw	25	30	22	24	22	22	25		26	20	20
# of lose/draw	22	5	14	10	15	12	9		5	13	17
rank test	0.217	0.000	0.071	0.003	0.044	0.004	0.001		0.000	0.011	0.106

C.3 Comparison with previously reported results

Although we compared various hyperparameter settings against the original paper to ensure as fair a comparison as possible, our results may not represent those in the original paper due to some differences in basic hyperparameter settings (e.g. fixing the learning rate to 0.001). Therefore, we compared our results with previously reported results, and the results are presented in Table 7.

Among the baseline models, only papers that directly evaluated the classification results are used and mentioned in the table. If multiple papers reported results for a particular model–dataset pair, the highest value was used for comparison. For Hydra and MR+Hydra, the results reported in BORF (Spinnato et al., 2024) were used. Note that we approximated the reported values using the number of test samples since they were typically rounded to one or two decimal places.

The metrics used in Table 7 are as follows:

- **report $\leq$ ours:** Count of datasets on which our experimental results of grid search achieved higher or equal accuracy compared to the reported results. A value higher than "report $\geq$ ours" indicates that existing reports likely underestimated the model.
- **report $\geq$ ours:** Count of datasets on which our experimental results of grid search achieved lower or equal accuracy compared to the reported results. A value higher than "report $\leq$ ours" indicates that our experiments likely underestimated the model.
- **acc difference:** Average difference between our experimental accuracy and the reported accuracy, calculated only for datasets with paired results. A positive number indicates that our experiments achieved higher accuracy, while a negative number indicates the opposite.

Table 7: Comparison of our experimental results and previous reported results.

(a) Comparison results on TSC-specific models.

	Distance		TSC-specific												
	DTW$_D$ (1994)		ROCKET (2020)		HC2 (2021)		Hydra (2023)		MR+Hydra (2023)		InterpGN (2025)		TSCMamba (2025)	
	TimesNet	**ours**	TimesNet TSLANet TSCMamba	**ours**	original	**ours**	BORF	**ours**	BORF	**ours**	original	**ours**	original	**ours**
EC	32.281	32.319	45.209	44.487	79.087	52.852	54.791	54.373	58.897	60.076	30.418	28.897	62.015	30.798
FD	52.900	52.866	64.699	61.606	71.348	61.379	52.301	60.982	61.901	61.294	66.402	63.791	69.401	70.204
HW	28.600	60.706	58.800	59.294	56.341	56.000	46.600	56.353	51.400	53.529	61.882	58.706	53.306	45.059
HB	71.707	71.707	75.610	75.610	72.878	78.537	76.098	76.585	73.220	77.073	79.512	80.488	76.585	78.537
JV	94.892	95.946	96.189	83.784		98.378	97.811	97.838	97.811	98.378	99.189	99.730	97.000	98.378
PEMS	71.098	71.098	75.087	84.393	99.827	97.688	80.289	98.266	77.514	82.659	88.439	86.127	90.173	90.173
SRS1	77.713	77.474	90.785	85.666	87.884	89.078	86.689	86.689	95.188	94.881	92.491	90.444	92.491	92.833
SRS2	53.889	53.889	54.444	55.556	50.444	54.444	58.889	58.889	56.722	55.000	57.778	58.333	66.722	62.222
SAD	96.298	97.226	99.200	99.227		99.136	98.899	99.136	99.300	99.045	99.818	99.864	99.000	95.816
UW	90.313	90.313	94.406	94.063	94.875	94.063	90.906	94.375	94.094	94.063	91.875	88.438	93.813	95.313
AWR		98.667	99.333	99.333	99.567	99.333	99.000	99.333	99.333	99.333	99.667	99.000	97.000	99.333
AF		20.000	20.000	6.667	28.000	20.000	13.333	26.667	6.667	6.667	33.333	46.667	67.333	66.667
BM		97.500	100.000	100.000	99.000	100.000	100.000	100.000	100.000	100.000	100.000	100.000	100.000	100.000
CT		98.816	98.753	99.304		99.304	98.600	99.164	99.199	99.373	99.791	99.791	98.997	99.513
CR		100.000	98.611	100.000	100.000	100.000	98.611	100.000	98.611	98.611	100.000	100.000	98.611	100.000
DDG		58.000	52.000	52.000	49.800	70.000	68.000	68.000	64.000	60.000	68.000	76.000	62.000	50.000
EW		61.832	78.626	91.603	89.466	97.710	98.473	98.473	96.183	98.473	83.969	82.443	87.023	88.550
EP		96.377	98.551	99.275	99.783	100.000	100.000	100.000	100.000	100.000	99.275	97.826	97.101	99.275
ER		91.481	94.074	98.889	98.519	98.889	98.519	98.889	98.889	99.259	95.185	87.778	91.519	97.037
FM		53.000	61.000	57.000	55.200	61.000	55.000	55.000	56.000	60.000	64.000	67.000	69.000	66.000
HMD		18.919	50.000	51.351	39.730	48.649	21.622	51.351	36.486	36.486	48.649	45.946	71.622	60.811
IW		48.692	10.000	38.524		66.796	67.900	67.052	66.700	65.744	66.752	67.180	14.300	68.244
LIB		87.222	83.889	90.556	92.667	94.444	93.278	93.333	92.778	93.333	97.222	97.222	90.000	91.667
LSST		55.109	54.100	64.031	63.694	66.383	60.702	66.504	63.601	64.274	60.665	59.570	60.300	60.057
MI		50.000	53.000	54.000	53.200	50.000	50.000	54.000	48.000	51.000	64.000	67.000	62.000	67.000
NATO		88.333	83.333	89.444	89.222	91.111	87.222	90.000	91.722	93.333	98.889	98.889	94.444	92.222
PD		97.713	97.341	98.228	99.557	97.656	96.801	97.856	96.801	97.284	99.142	99.342	98.542	98.513
PS		15.121	17.599	27.826	29.427	33.015	32.401	33.164	35.401	33.642	32.180	33.075	24.659	23.800
RS		80.263	86.184	90.789	93.026	90.132	91.382	91.447	90.789	90.132	90.789	91.447	91.447	90.789
SWJ		20.000	46.667	46.667	44.000	40.000	40.000	40.000	60.000	66.667	53.333	60.000	73.333	73.333
report $\leq$ ours	8		23		15		28		21		18		17	
report $\geq$ ours	6		12		12		10		15		17		16	
acc difference	3.385		2.056		0.224		3.320		0.747		0.278		0.080	

Table 7: *(Continued.)* Comparison of our experimental results and previous reported results.

(b) Comparison results on foundation models.

	Foundation													
	TimesNet (2023)			ModernTCN (2024)			TSLANet (2024)			TimeMixer++ (2025a)		GPT4TS (2023)		
	original	TSLANet TSCMamba	**ours**	original	revisit	**ours**	original	TSCMamba	**ours**	original	**ours**	original	TSLANet TSCMamba	**ours**
EC	35.703	27.719	33.460	36.312	31.901	32.319	30.418		31.939	39.886	34.601	34.183	25.475	32.319
FD	68.601	67.469	70.148	70.800	68.700	66.998	66.771		66.969	71.799	69.665	69.200	65.579	68.615
HW	32.106	26.176	37.529	30.600	28.400	30.118	57.882		62.000	26.506	33.647	32.706	3.765	34.118
HB	78.000	74.488	83.902	77.220	77.122	78.049	77.561		79.512	79.122	80.488	77.220	36.585	79.024
JV	98.405	97.838	98.649	98.811	98.108	98.649	99.189		98.919	97.892	99.189	98.595	98.108	98.108
PEMS	89.595	88.150	87.861	89.075	83.179	86.705	83.815		89.017	90.983	89.017	87.919	87.283	88.439
SRS1	91.809	77.440	92.150	93.413	92.799	93.515	91.809		89.761	93.106	92.150	93.208	91.468	93.174
SRS2	57.222	52.833	60.000	60.278	61.722	60.000	61.667		63.889	65.611	60.556	59.389	51.667	60.556
SAD	99.000	98.358	99.545	98.699	98.099	99.500	99.909		98.045	99.800	99.545	99.200	99.363	99.591
UW	85.313	83.125	88.438	86.688	85.906	88.438	91.250		94.375	88.188	90.625	88.094	84.375	89.063
AWR		96.167	98.667			98.667	99.000		99.333		99.000		93.333	98.667
AF		33.333	66.667			73.333	40.000		66.667		66.667		33.333	66.667
BM		100.000	100.000			100.000	100.000		100.000		100.000		92.500	100.000
CT		97.981	98.747			99.304		98.747	99.164		99.373		98.259	99.373
CR		87.500	97.222			97.222	98.611		91.667		98.611		8.333	97.222
DDG		56.000	68.000			66.000		24.000	74.000		74.000		50.000	66.000
EW		58.779	63.359			64.122		41.221	81.679		61.069		48.092	66.412
EP		78.116	96.377			96.377	98.551		100.000		94.928		85.507	89.855
ER		94.074	95.556			97.407		91.481	85.926		96.296		95.926	96.296
FM		59.400	66.000			67.000	61.000		68.000		67.000		57.000	66.000
HMD		50.000	72.973			66.216	52.703		48.649		72.973		18.919	70.270
IW		10.000	64.024			75.588	10.000		10.012		64.192		10.000	61.396
LIB		77.833	88.333			90.000	92.778		95.556		88.333		79.444	87.778
LSST		59.209	44.120			43.593	66.338		51.014		44.444		46.391	38.078
MI		51.000	68.000			67.000	62.000		71.000		67.000		50.000	67.000
NATO		81.833	98.333			95.556	95.556		99.444		96.111		91.667	96.111
PD		98.190	98.914			98.513	98.939		99.028		98.599		97.742	98.513
PS		18.240	14.524			13.749	17.751		4.921		15.508		3.012	13.123
RS		82.632	89.474			84.211	90.789		94.079		91.447		76.974	86.842
SWJ		53.333	66.667			80.000	46.667		73.333		73.333		33.333	73.333
report ≤ ours	8	27		4	8		19	3		4		6	29	
report ≥ ours	2	4		6	2		8	1		6		4	2	
acc difference	1.593	9.014		(0.761)	0.835		2.161	21.330		(0.341)		0.330	15.617	

(c) Comparison results on TSF-origin models.

	TSF-origin															
	DLinear (2023)		LightTS (2022)		MTS-Mixer (2023)		FEDformer (2022)		ETSformer (2022)		Crossformer (2023)		PatchTST (2023)		iTransformer (2024)	
	TimesNet TSLANet TSCMamba	**ours**	TimesNet	**ours**	ModernTCN	**ours**	TimesNet	**ours**	TimesNet	**ours**	ModernTCN TSLANet TSCMamba	**ours**	ModernTCN TSLANet TSCMamba	**ours**	TimeMixer++	**ours**
EC	33.460	31.179	29.696	32.319	33.802	30.798	31.217	33.840	28.099	33.080	37.985	43.346	32.814	32.700	28.099	31.939
FD	67.999	69.495	67.500	68.473	70.199	68.530	65.999	69.892	66.300	68.331	68.700	69.637	68.961	68.076	66.300	68.417
HW	27.000	23.765	26.106	25.059	26.000	19.647	28.000	33.412	32.506	35.647	28.800	30.353	29.600	29.529	24.200	31.294
HB	75.122	76.585	75.122	77.561	77.122	79.024	73.707	78.049	71.220	78.537	77.610	79.024	76.585	73.659	75.610	78.049
JV	97.838	96.486	96.189	96.757	94.297	95.946	98.405	97.568	95.892	98.378	99.108	98.378	98.649	97.027	96.595	98.108
PEMS	82.081	82.659	88.382	87.861	80.925	82.081	80.925	89.017	86.012	87.861	85.896	89.595	89.306	89.017	87.919	91.329
SRS1	88.396	92.833	89.795	92.833	91.706	78.840	88.703	75.085	89.590	92.150	92.491	93.857	90.717	89.078	90.205	93.857
SRS2	51.667	57.222	51.111	59.444	55.000	58.333	54.389	59.444	55.000	60.000	58.278	61.667	57.778	61.667	54.389	58.889
SAD	96.680	96.953	100.000	98.226	97.399	99.454	100.000	99.454	100.000	99.000	97.899	98.863	99.682	98.818	95.998	99.318
UW	82.094	82.813	80.313	89.063	82.313	83.125	85.313	79.688	85.000	89.688	85.313	88.438	85.813	89.375	85.906	90.000
AWR	97.333	97.667		98.333		99.000		92.333		98.667	98.000	98.667	97.667	98.667		99.000
AF	46.667	53.333		73.333		60.000		73.333		80.000	46.667	73.333	53.333	80.000		66.667
BM	85.000	87.500		100.000		100.000		95.000		100.000	90.000	100.000	92.500	85.000		97.500
CT	97.347	98.120		98.955		97.981		97.284		98.468	98.329	98.955	97.347	98.398		98.886
CR	91.667	91.667		93.056		97.222		90.278		98.611	84.722	97.222	84.722	97.222		97.222
DDG	62.000	66.000		56.000		68.000		42.000		42.000	44.000	72.000	24.000	40.000		60.000
EW	41.221	42.748		54.198		66.412		63.359		70.992	54.962	58.015	54.198	57.252		59.542
EP	60.145	65.217		97.101		66.667		92.754		92.754	73.188	95.652	65.942	98.551		80.435
ER	91.481	91.852		94.444		77.778		95.926		96.296	94.074	97.407	92.593	96.667		94.815
FM	64.000	62.000		64.000		63.000		72.000		66.000	64.000	64.000	62.000	63.000		64.000
HMD	58.108	66.216		66.216		70.270		71.622		63.514	58.108	66.216	58.108	63.514		58.108
IW	10.000	18.996		71.676		72.424		65.244		64.868	10.000	73.712	10.000	60.936		72.456
LIB	73.333	70.556		89.444		34.444		93.333		90.000	76.111	90.556	81.111	81.667		91.667
LSST	35.770	34.023		41.525		34.185		40.998		41.241	42.818	41.768	67.798	56.732		40.673
MI	61.000	64.000		68.000		66.000		65.000		67.000	61.000	68.000	61.000	69.000		67.000
NATO	93.889	96.111		97.222		95.000		96.111		93.333	88.333	93.889	96.667	80.556		88.889
PD	92.939	92.481		96.998		46.941		98.599		98.542	93.651	98.513	99.231	98.485		98.428
PS	7.101	6.651		16.224		5.428		11.691		14.316	7.551	14.256	11.691	15.091		11.542
RS	78.947	78.947		81.579		86.842		84.868		85.526	81.579	87.500	84.211	85.526		81.579
SWJ	60.000	53.333		73.333		66.667		66.667		66.667	53.333	80.000	60.000	86.667		73.333
report ≤ ours	21		7		6		6		9		28		18		10	
report ≥ ours	11		3		4		4		1		3		12		0	
acc difference	1.237		2.338		(1.298)		0.879		3.305		9.010		5.262		3.598	

C.4 Visualization of time variance ablation

Figure 9 shows visualizations of MambaSL's classification accuracy results on the UEA benchmark, tested for various hyperparameter combinations along with TI/TV configurations. Among 240 combinations, 10 sets of hyperparameter combinations that showed high performance regardless of the TI/TV configurations were selected (8×10=80 in total) and depicted in box and line plots. Each line represents the same hyperparameter settings except for time variance configurations.

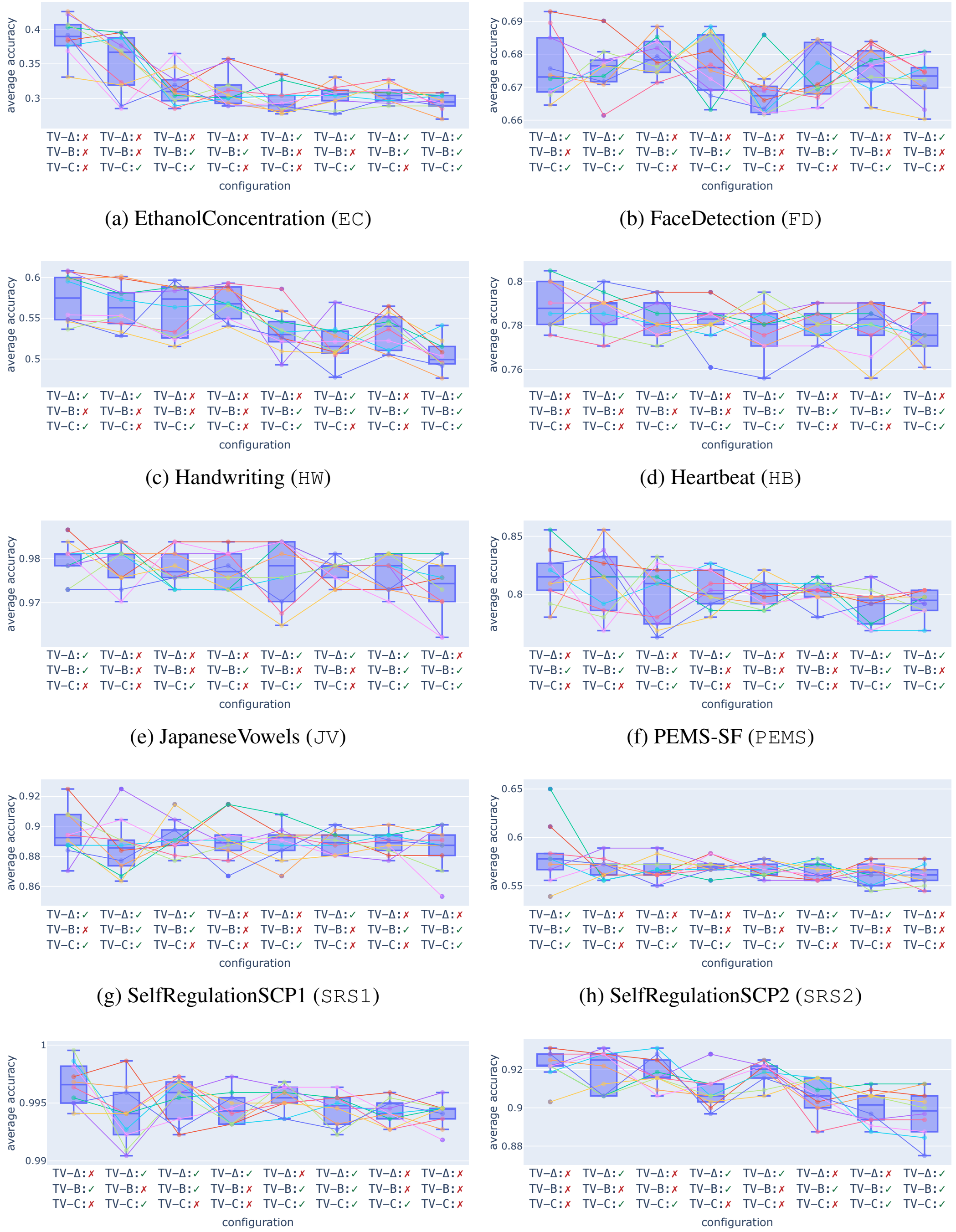

(a) EthanolConcentration (EC)

(b) FaceDetection (FD)

(c) Handwriting (HW)

(d) Heartbeat (HB)

(e) JapaneseVowels (JV)

(f) PEMS-SF (PEMS)

(g) SelfRegulationSCP1 (SRS1)

(h) SelfRegulationSCP2 (SRS2)

(i) SpokenArabicDigits (SAD)

(j) UWaveGestureLibrary (UW)

Figure 9: Visualization of classification accuracy of MambaSL along TI/TV configurations on the UEA benchmark, in order of maximum accuracy.

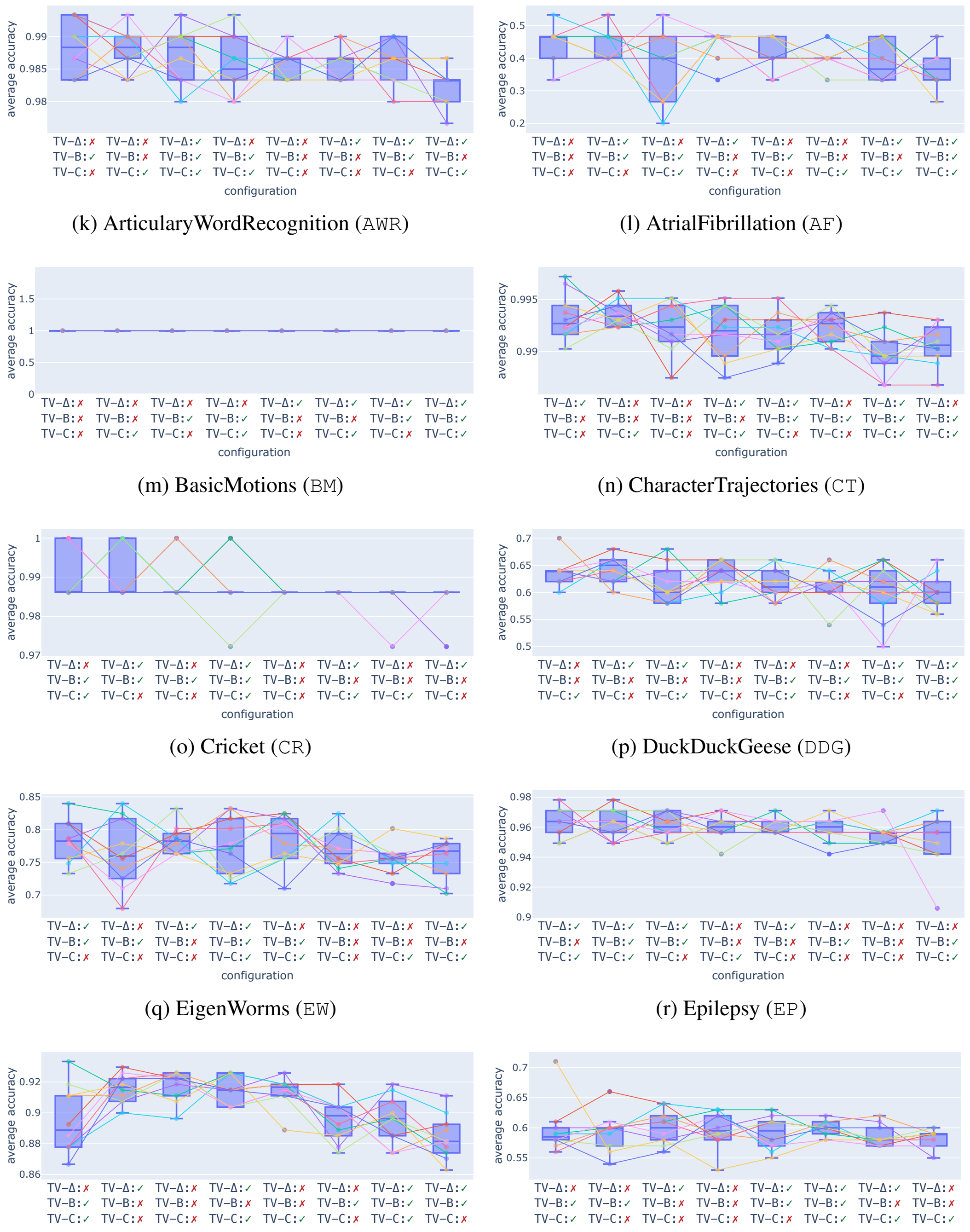

(k) ArticularyWordRecognition (`AWR`)

(l) AtrialFibrillation (`AF`)

(m) BasicMotions (`BM`)

(n) CharacterTrajectories (`CT`)

(o) Cricket (`CR`)

(p) DuckDuckGeese (`DDG`)

(q) EigenWorms (`EW`)

(r) Epilepsy (`EP`)

(s) ERing (`ER`)

(t) FingerMovements (`FM`)

Figure 9: *(Continued.)* Visualization of classification accuracy of MambaSL along TI/TV configurations on the 30 UEA datasets, in order of maximum accuracy.

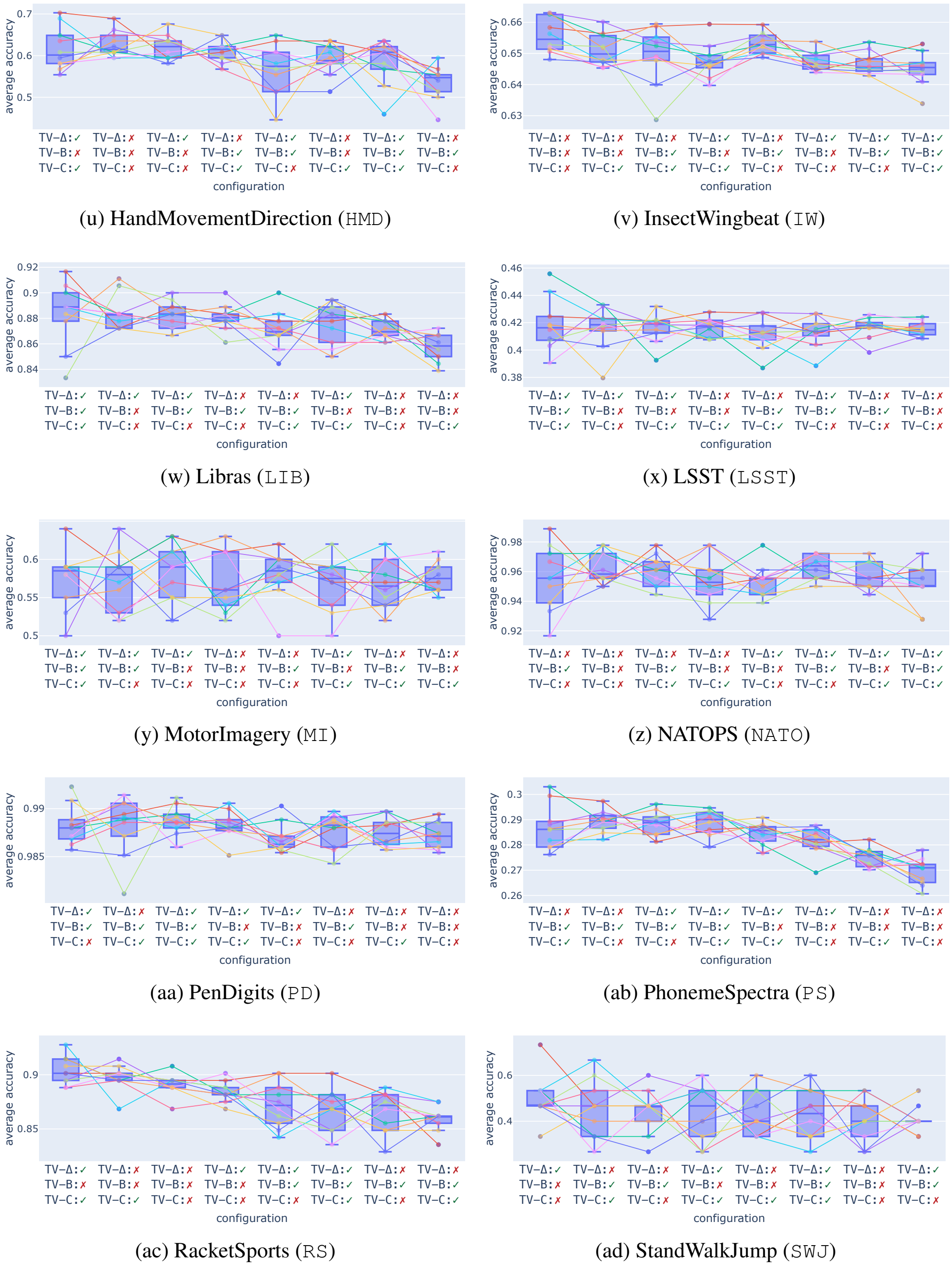

(u) HandMovementDirection (HMD)

(v) InsectWingbeat (IW)

(w) Libras (LIB)

(x) LSST (LSST)

(y) MotorImagery (MI)

(z) NATOPS (NATO)

(aa) PenDigits (PD)

(ab) PhonemeSpectra (PS)

(ac) RacketSports (RS)

(ad) StandWalkJump (SWJ)

Figure 9: *(Continued.)* Visualization of classification accuracy of MambaSL along TI/TV configurations on the 30 UEA datasets, in order of maximum accuracy.

C.5 Full results of MambaSL performance according to model depth

Table 8 presents the complete comparison results corresponding to Table 3. Although using three layers yielded the highest average accuracy on the 10 datasets commonly evaluated in `TSLib`, this observation does not hold when extended to the full set of 30 UEA datasets. When examining the average rank on these 10 datasets, we find that the single-layer configuration consistently outperforms the multi-layer variants, indicating that the higher average accuracy for deeper models is driven by a small subset of datasets. In particular, the `HW` dataset exhibits a nearly 5%p improvement with 2–3 layers compared to a single layer, which disproportionately affects the average accuracy metric.

Table 8: Classification accuracy (%) of MambaSL according to its model depth on 30 datasets from the UEA archives. The best and the second-best are highlighted in bold and underline, respectively.

	model depth		
	1 (proposed)	2	3
EC	42.586	41.065	41.825
FD	69.296	68.785	69.098
HW	60.824	65.765	66.353
HB	80.488	80.488	80.488
JV	98.649	98.649	98.378
PEMS	85.549	85.549	86.705
SRS1	92.491	92.150	91.126
SRS2	65.000	62.778	62.222
SAD	99.955	99.864	99.864
UW	93.438	93.438	93.125
AWR	99.333	99.333	99.333
AF	53.333	53.333	60.000
BM	100.000	100.000	100.000
CT	99.721	99.652	99.721
CR	100.000	100.000	100.000
DDG	70.000	70.000	68.000
EW	83.969	83.206	85.496
EP	97.826	97.826	97.101
ER	93.704	95.185	94.074
FM	71.000	67.000	65.000
HMD	70.270	68.919	68.919
IW	66.304	64.772	65.596
LIB	91.667	91.111	89.444
LSST	45.580	44.039	42.539
MI	69.000	67.000	66.000
NATO	98.889	98.889	98.333
PD	99.257	99.171	99.200
PS	30.331	31.435	30.987
RS	92.763	93.421	92.763
SWJ	73.333	66.667	66.667
avg. acc (10)	78.827	78.853	**78.918**
avg. acc	**79.819**	79.316	79.279
avg. rank (10)	**1.30**	1.90	2.10
avg. rank	**1.33**	1.80	2.07
# of win/draw		26	24
# of lose/draw		15	12
rank test		0.035	0.004

C.6 Classification results on the UEA benchmark under InceptionTime setting

To address the data-leakage concern raised for `TSLib`, we trained MambaSL under the InceptionTime protocol, which selects the checkpoint with the lowest training loss (Ismail Fawaz et al., 2020). For comparison, we selected the top three high-performing models from each source—HC2 (Middlehurst et al., 2021), BORF (Spinnato et al., 2024), and our own experiments—to form a representative conventional TSC baseline set. For HC2, we used only the results from fold 0, the official train–test split[3], and for BORF, we approximated the reported accuracies using the number of test samples as described in appendix C.3.

Table 9 summarizes the results. Although MambaSL achieved slightly lower average accuracy than HC2 and Hydra, it remained competitive, achieving the largest number of top-1 results (15 datasets) and outperforming every non-DL baseline in direct head-to-head comparisons. These findings indicate that MambaSL maintains strong performance under leakage-free model selection.

Since all experimental hyperparameters and optimization settings were fixed to the same values as in our original experiments, the performance differences between Tables 5 and 9 arise solely from the change in the model selection criterion.

Table 9: UEA classification accuracy (%) of MambaSL using the InceptionTime protocol (selecting the checkpoint with the lowest training loss). The comparison set includes the top three models from each HC2 (Middlehurst et al., 2021), BORF (Spinnato et al., 2024), and our own evaluations. The best and the second-best are highlighted in bold and underline, respectively.

	HC2 reported (2021)			BORF reported (2024)			our experiments			
	CIF (2020)	DrCIF (2021)	HC2 (2021)	Mini Rocket (2021)	DrCIF (2021)	MR+ Hydra (2023)	HC2 (2021)	Hydra (2023)	MR+ Hydra (2023)	**MambaSL (proposed)**
EC	73.384	69.202	**77.186**	48.289	63.118	58.935	52.852	54.373	60.076	39.163
FD	62.713	62.003	66.033	58.201	59.109	61.890	61.379	60.982	61.294	**68.331**
HW	35.647	34.588	54.824	51.765	36.235	51.412	56.000	56.353	53.529	**59.294**
HB	78.049	**79.024**	73.171	74.146	**79.024**	73.171	78.537	76.585	77.073	76.585
JV				**99.189**	97.297	97.838	98.378	97.838	98.378	98.649
PEMS	**100.000**	**100.000**	**100.000**	82.659	**100.000**	77.457	97.688	98.266	82.659	83.237
SRS1	86.007	87.713	89.078	91.809	87.031	**95.222**	89.078	86.689	94.881	88.737
SRS2	50.000	49.444	50.000	54.444	51.111	56.667	54.444	58.889	55.000	**61.111**
SAD				99.318	97.817	99.318	99.136	99.136	99.045	**99.727**
UW	92.500	90.938	92.813	93.125	93.750	94.063	94.063	**94.375**	94.063	92.500
AWR	98.333	98.000	**99.333**	**99.333**	**99.333**	**99.333**	**99.333**	**99.333**	**99.333**	**99.333**
AF	33.333	33.333	26.667	13.333	40.000	6.667	20.000	26.667	6.667	**46.667**
BM	**100.000**	**100.000**	**100.000**	**100.000**	**100.000**	**100.000**	**100.000**	**100.000**	**100.000**	**100.000**
CT				99.304	98.120	99.234	99.304	99.164	99.373	**99.582**
CR	98.611	98.611	**100.000**	98.611	98.611	98.611	**100.000**	**100.000**	98.611	**100.000**
DDG	44.000	54.000	56.000	**70.000**	48.000	64.000	**70.000**	68.000	60.000	**70.000**
EW	91.603	92.366	94.656	93.893	93.130	96.183	97.710	**98.473**	**98.473**	83.206
EP	98.551	97.826	**100.000**	**100.000**	**100.000**	**100.000**	**100.000**	**100.000**	**100.000**	97.826
ER	98.148	**99.259**	98.889	97.778	**99.259**	98.889	98.889	98.889	**99.259**	92.593
FM	52.000	60.000	53.000	57.000	47.000	56.000	61.000	55.000	60.000	**64.000**
HMD	59.459	52.703	47.297	39.189	51.351	36.486	48.649	51.351	36.486	**62.162**
IW				**67.300**	66.400	66.700	66.796	67.052	65.744	64.524
LIB	91.111	89.444	93.333	91.667	89.444	92.778	**94.444**	93.333	93.333	90.556
LSST	57.259	55.596	64.274	65.085	56.488	63.585	66.383	**66.504**	64.274	25.182
MI	50.000	44.000	54.000	50.000	50.000	48.000	50.000	54.000	51.000	**62.000**
NATO	85.556	84.444	89.444	94.444	82.778	91.667	91.111	90.000	93.333	**98.889**
PD	96.741	97.656	97.913		97.313	96.798	97.656	97.856	97.284	**99.228**
PS	26.543	30.778	29.049	29.407	**39.994**	35.401	33.015	33.164	33.642	29.824
RS	88.158	90.132	90.789	85.526	88.816	90.789	90.132	**91.447**	90.132	90.789
SWJ	40.000	53.333	46.667	40.000	40.000	60.000	40.000	40.000	**66.667**	60.000
# of win/draw	18	19	17	19	20	20	18	19	18	
# of lose/draw	10	9	13	13	12	14	16	15	14	
rank test	0.081	0.088	0.173	0.046	0.072	0.082	0.307	0.240	0.221	
acc difference	2.058	1.416	(0.123)	2.061	1.777	1.218	(0.076)	(0.334)	0.470	

[3] The full set of reported results is available at timeseriesclassification.com.

The higher performance observed in our re-evaluation of certain non-DL baselines in Table 9 stems from running three random seeds and reporting the best-performing run. Using only a single seed (seed 0) yields results comparable to those originally reported for HC2 and BORF.

To further assess stability, we conducted two additional trials for MambaSL and report the mean and standard deviation across three trials in Table 10.

In contrast to Table 9, where HC2 and Hydra showed the strongest performance based on the best-performing trial, averaging across all trials indicates that MR+Hydra achieves the strongest mean performance and exhibits more consistent results. Nevertheless, MambaSL remains competitive, outperforming all conventional non-DL baselines in direct head-to-head comparisons and achieving the largest number of top-1 results (13 datasets). The Wilcoxon signed-rank test indicates no significant difference between MambaSL and MR+Hydra, suggesting comparable overall effectiveness under this protocol.

Table 10: Mean and standard deviation of UEA classification accuracy (%) of MambaSL using the InceptionTime protocol (selecting the checkpoint with the lowest training loss). The comparison set includes the four non-DL models from our own evaluations. The best and the second-best are highlighted in bold and underline, respectively.

	our experiments				
	ROCKET (2020)	HC2 (2021)	Hydra (2023)	MR+Hydra (2023)	**MambaSL** **(proposed)**
EC	**99.333 ±0.000**	99.111 ±0.385	99.222 ±0.192	99.222 ±0.192	99.111 ±0.385
FD	6.667 ±0.000	17.778 ±3.849	17.778 ±7.698	6.667 ±0.000	**42.222 ±7.698**
HW	**100.000 ±0.000**	**100.000 ±0.000**	**100.000 ±0.000**	**100.000 ±0.000**	**100.000 ±0.000**
HB	99.257 ±0.040	98.793 ±0.464	99.071 ±0.106	99.327 ±0.040	**99.513 ±0.070**
JV	**100.000 ±0.000**	99.537 ±0.802	99.537 ±0.802	98.611 ±0.000	**100.000 ±0.000**
PEMS	48.667 ±3.055	59.333 ±13.614	50.000 ±19.079	56.667 ±3.055	**65.333 ±6.429**
SRS1	90.331 ±1.166	94.402 ±4.473	93.639 ±4.341	**97.201 ±1.166**	82.188 ±1.166
SRS2	98.792 ±0.418	**100.000 ±0.000**	**100.000 ±0.000**	**100.000 ±0.000**	97.343 ±0.837
SAD	98.642 ±0.428	98.395 ±0.566	**98.765 ±0.214**	98.395 ±0.932	91.728 ±1.497
UW	42.966 ±1.742	50.824 ±3.189	50.190 ±3.627	**58.175 ±2.662**	37.896 ±1.335
AWR	61.076 ±0.512	55.789 ±4.842	57.454 ±4.565	60.036 ±1.122	**67.263 ±0.928**
AF	55.000 ±2.000	55.333 ±6.028	53.667 ±2.309	**59.333 ±1.155**	58.667 ±6.807
BM	49.550 ±3.121	36.486 ±10.554	38.739 ±15.368	34.234 ±2.064	**63.514 ±2.341**
CT	**58.863 ±0.378**	49.451 ±5.831	53.098 ±5.335	52.588 ±0.941	58.667 ±1.087
CR	74.472 ±1.228	**76.260 ±2.200**	75.772 ±1.015	75.610 ±1.291	72.683 ±3.683
DDG	38.348 ±0.189	64.677 ±3.635	61.279 ±5.004	**65.692 ±0.074**	64.264 ±0.227
EW	82.883 ±0.780	94.324 ±7.022	90.270 ±6.642	97.928 ±0.563	**98.198 ±0.780**
EP	90.185 ±0.321	93.148 ±1.398	92.222 ±0.962	**93.333 ±0.000**	89.815 ±1.283
ER	63.869 ±0.247	62.693 ±3.199	**64.355 ±3.145**	63.328 ±1.071	18.194 ±6.194
FM	51.667 ±2.082	47.667 ±4.041	52.000 ±2.000	50.333 ±0.577	**60.667 ±4.163**
HMD	88.333 ±1.111	89.074 ±1.951	88.333 ±1.470	91.481 ±1.604	**97.778 ±1.470**
IW	83.815 ±0.578	85.356 ±10.927	**91.908 ±10.029**	80.539 ±2.030	82.659 ±3.218
LIB	98.132 ±0.100	96.884 ±0.722	97.484 ±0.619	97.170 ±0.103	**99.123 ±0.259**
LSST	27.378 ±0.517	31.663 ±1.849	31.057 ±1.827	**32.995 ±0.707**	28.780 ±1.002
MI	**90.789 ±0.000**	87.939 ±2.310	**90.789 ±0.658**	89.035 ±1.005	89.912 ±1.519
NATO	85.324 ±0.341	87.827 ±1.097	86.121 ±0.710	**94.084 ±0.859**	87.372 ±2.365
PD	52.407 ±3.349	52.407 ±1.786	54.630 ±4.170	53.889 ±0.962	**56.667 ±4.194**
PS	99.151 ±0.131	98.530 ±0.533	98.909 ±0.355	98.939 ±0.095	**99.576 ±0.131**
RS	46.667 ±0.000	37.778 ±3.849	40.000 ±0.000	**57.778 ±15.396**	53.333 ±11.547
SWJ	93.646 ±0.477	92.188 ±1.740	93.021 ±2.081	**93.750 ±0.541**	91.979 ±0.902
# of win/draw	18	18	18	16	
# of lose/draw	14	14	13	15	
rank test	0.127	0.169	0.185	0.461	
acc difference	2.608	1.360	1.171	(0.063)	

C.7 Classification results on ADFTD and FLAAP

While the UEA archive provides a standardized benchmark for multivariate TSC, it mainly consists of datasets released between 1999 and 2018, many of which are relatively clean and small in scale (Bagnall et al., 2018). To evaluate the robustness of our model beyond these settings, we additionally tested MambaSL on two more recent and domain-specific TSC datasets.

Following the evaluation protocol of Medformer (Wang et al., 2024a), we selected ADFTD (Miltiadous et al., 2023) from the medical domain and FLAAP (Kumar & Suresh, 2022) from the human activity recognition (HAR) domain. A summary of both datasets is provided in Table 11.

Table 11: Summary of ADFTD and FLAAP datasets

Dataset	Domain	Samples	Length	Variables	Classes	File Size
ADFTD (2023)	EEG	69752	256	3	19	2.52GB
FLAAP (2022)	HAR	13123	100	10	6	60.2MB

Preprocessing and experimental settings were aligned with the official Medformer implementation. We first evaluated MambaSL using the 240 hyperparameter configurations employed for the UEA experiments, after which we conducted four additional trials on some best-performing configurations, resulting in a total of five runs. Table 12 reports the average accuracy and F1-score across these trials. For comparison, we also include the results of the strongly performing baselines reported by Medformer (Wang et al., 2024a): Crossformer (Zhang & Yan, 2023), Reformer (Kitaev et al., 2020), Transformer (Vaswani et al., 2017), TCN (Bai et al., 2018), ModernTCN (Luo & Wang, 2024), and Mamba (Gu & Dao, 2024). Since the original Medformer paper did not report results for TCN, ModernTCN, and Mamba on ADFTD, these entries are left blank.

As shown in Table 12, MambaSL performed competitively against previous baselines on both datasets, and achieved the highest accuracy on FLAAP. In particular, we observe more than a 10%p improvement over the vanilla Mamba. Taken together, the results on ADFTD and FLAAP show that MambaSL remains stable across domains and dataset scales, reinforcing that its performance is not limited to the characteristics of the UEA archive.

Table 12: Classification accuracy and F1-score (%) of MambaSL and other baselines on ADFTD and FLAAP datasets. The best and the second-best are highlighted in bold and underline, respectively.

	ADFTD		FLAAP	
	accuracy	F1-score	accuracy	F1-score
Crossformer (2023)	50.45 ±2.31	45.50 ±1.70	75.84 ±0.52	75.52 ±0.66
Reformer (2020)	50.78 ±1.17	47.94 ±1.59	71.65 ±1.27	71.14 ±1.45
Transformer (2017)	50.47 ±2.14	48.09 ±1.59	74.96 ±1.25	74.49 ±1.39
TCN (2018)			66.48 ±1.66	65.29 ±1.74
ModernTCN (2024)			74.80 ±0.96	74.35 ±0.85
Mamba (2024)			64.87 ±2.78	64.14 ±2.70
Medformer (2024a)	**53.27 ±1.54**	**50.65 ±1.51**	76.44 ±0.64	76.25 ±0.65
MambaSL (proposed)	51.68 ±0.89	48.73 ±3.05	**77.47 ±1.03**	**77.59 ±1.15**